UNIVERSITY OF CALIFORNIA

Santa Barbara

Heightened Delivery of Silica to Cretaceous Seas, the Fossil Record of Silica Biomineralization, and the Search for a Seawater Silica Proxy

A Thesis submitted in partial satisfaction of the

requirements for the degree Master of Science

in Geological Sciences

by

Abby Leigh Wyant

Committee in charge:

Professor Frank Spera, Chair

Professor Stanley Awramik

Professor Susannah Porter

December 2015

The dissertation of Abby Leigh Wyant is approved.

_____

Stan Awramik

_____

Susannah Porter

_____

Frank Spera, Committee Chair

December 2015

ACKNOWLEDGEMENTS

I would like to thank my thesis committee members Frank Spera, Susannah Porter, and Stan Awramik for their generous help and support, which made this thesis possible. I would like to especially thank Frank Spera and Susannah Porter. I would like to thank Frank for advising on the geochemical portion of this thesis, with which he generously gave his time, encouragement, and support. I would like to thank Susannah for advising on the paleontology aspect of this thesis and helping to conceive its research topic. I thank both advisors for making my time at the University of California, Santa Barbara such a challenging and fun experience. I would like to thank all of my committee members for their feedback on this manuscript, their comments improved its clarity and quality. I would also like to thank John Cottle, Alex Simms, David Lea, Jake Poletti, Michael Bentz, John Moore, and Gareth Seward for their generous help at various times throughout my graduate career. I thank my parents, Diane Wyant and Lee Wyant, for their continual encouragement and support during these last two years. Lastly, I would not like to thank the Epstein Barr virus and *Streptococcus pneumoniae* for their extended stay in my body during the summer of 2015, but I would like to thank Mary McGuire for nursing me back to health. It is thanks to her care and support that I was able to finish my thesis in December of 2015.

ABSTRACT

Heightened Delivery of Silica to Cretaceous Seas, the Fossil Record of Silica Biomineralization, and the Search for a Seawater Silica Proxy

by

Abby Leigh Wyant

Silica biomineralization first appeared in the Cambrian with the appearances of siliceous sponges and polycystinean radiolarians, yet most siliceous taxa with a fossil record did not appear until the Cretaceous, about three hundred million years later. Contemporaneous seawater chemistry may have influenced the acquisition of a siliceous skeleton during the Cretaceous. Cretaceous seawater may have had elevated silica concentrations due to enhanced hydrothermal fluxes from fast spreading rates at mid-ocean ridges and the emplacement of voluminous ocean basin flood basalt provinces on the seafloor. In addition, heightened riverine runoff and warm temperatures may have also increased the delivery of silica to seawater by enhancing continental weathering. A proxy for tracing silica fluxes from continental weathering was undertaken by performing linear regression analyses on dissolved silica with other dissolved cations and polyanions reported in riverine runoff. No proxy for tracing global riverine silica fluxes to the ocean was identified. For rivers draining predominantly one type of lithology, however, dissolved Na^+ was found to strongly correlate with silica in rivers draining granitoid rocks

Linear regression analyses were performed on hydrothermal vent fluid datasets and a strong correlation between silica and strontium concentrations was found. When coupled with the $^{87}Sr/^{86}Sr$ seawater record, the correlation in hydrothermal vent fluids has great potential as a silica proxy. The $^{87}Sr/^{86}Sr$ record was therefore explored as a potential silica proxy. Two models are presented that attempt to explain the seawater $^{87}Sr/^{86}Sr$ curve: the first is a simple mixing model from Faure et al. (1965) that describes the $^{87}Sr/^{86}Sr$ value of the ocean as a result from the mixing of weathering products from three sources, each with a distinct $^{87}Sr/^{86}Sr$ value. The second model is from Brass (1976), which shows the rate of change in the $^{87}Sr/^{86}Sr$ seawater record is caused from variations in the fluxes of strontium from the weathering of carbonates and non-carbonates, each with a distinct $^{87}Sr/^{86}Sr$ value. A third, hydrothermal component was added to this model. Neither model is able to accurately explain the $^{87}Sr/^{86}Sr$ curve through time and therefore the $^{87}Sr/^{86}Sr$ is not a good candidate as a seawater silica proxy. Based on all available evidence, the hypothesis that high silica availability in Cretaceous seawater was a trigger for the first appearances of several siliceous taxa and the diversification of diatoms cannot be rejected. Further testing on the release of silica from ocean basin magmatic processes is required to further corroborate the link between silica biomineralization and heightened silica fluxes to Cretaceous seas.

I. Introduction

The Cretaceous Period (145 – 66 Ma) was a unique time in the history of skeletonized taxa. Several siliceous groups first appeared in the fossil record during the Cretaceous, following the earlier first appearance of siliceous sponges and polycystinean radiolarians during the Cambrian. The ocean basin magmatic processes of the Cretaceous were also unique, with heightened oceanic crust production and the concomitant emplacement of voluminous ocean basin flood basalt provinces. These events have been linked to a decrease in the heat flux emanating from the core that led to a 42-million-year span without geomagnetic reversals known as the Cretaceous Normal Polarity Superchron (125 – 83 Ma; Olson & Amit, 2015). In this study, the link between Earth's geologic processes and its influence on life is explored by determining if silica fluxes to Cretaceous seas were heightened, driving the independent acquisition of a siliceous skeleton seen in several groups during this period. It is hypothesized that Cretaceous seas were rich in silica derived from ocean basin and terrestrial sources, causing silica to be a favorable material for skeletal construction. The modern silica sources are discussed and applied to the geologic past with an emphasis on seafloor activity and continental weathering. Lastly, a search for a silica proxy is undertaken in an attempt to better constrain ancient silica fluxes to seawater. Linear regressions of silica concentrations with other reported variables in riverine water and hydrothermal vent fluids are presented in an attempt to find a correlation with silica from these sources. Lastly, the robust seawater $^{87}Sr/^{86}Sr$ curve is explored as a silica proxy. A simple, older model from Faure et al. (1965) is first presented. It attempts to explain the $^{87}Sr/^{86}Sr$ value of seawater from the mixing of weathering products from three sources, each with a distinct $^{87}Sr/^{86}Sr$ value. A more recent and complex model created by Brass (1976)

is then presented. This model explains that the rate of change in the $^{87}Sr/^{86}Sr$ seawater record is from variations in the fluxes of strontium from the weathering of carbonates and non-carbonates, each with a distinct $^{87}Sr/^{86}Sr$ value. A third, hydrothermal component was added to this model. These models are discussed in detail to determine if the $^{87}Sr/^{86}Sr$ record may be a viable seawater silica proxy.

II. The Fossil Record of Siliceous Taxa

The first appearance of polycystinean radiolarians during the Cambrian (Braun et al., 2007; Cao et al., 2014; Won & Below, 1999) is largely agreed upon, whereas the first appearance of siliceous sponges is currently debated. Unambiguous siliceous sponge body fossils first appear in the Cambrian (Xiao et al., 2005; Bengtson et al., 1990), yet controversial claims of body fossils have been reported from the Ediacaran (Gehling & Rigby, 1996; Braiser et al., 1997; Maloof et al., 2010; Brain et al., 2012; Yin et al., 2015). In addition, molecular clock estimates (Peterson et al., 2008) and biomarkers (Love et al., 2009) suggest a Cryogenian (720 - 635 Ma) origin (Sperling et al., 2010). A Cambrian first appearance of siliceous sponges is considered here as the best working hypothesis.

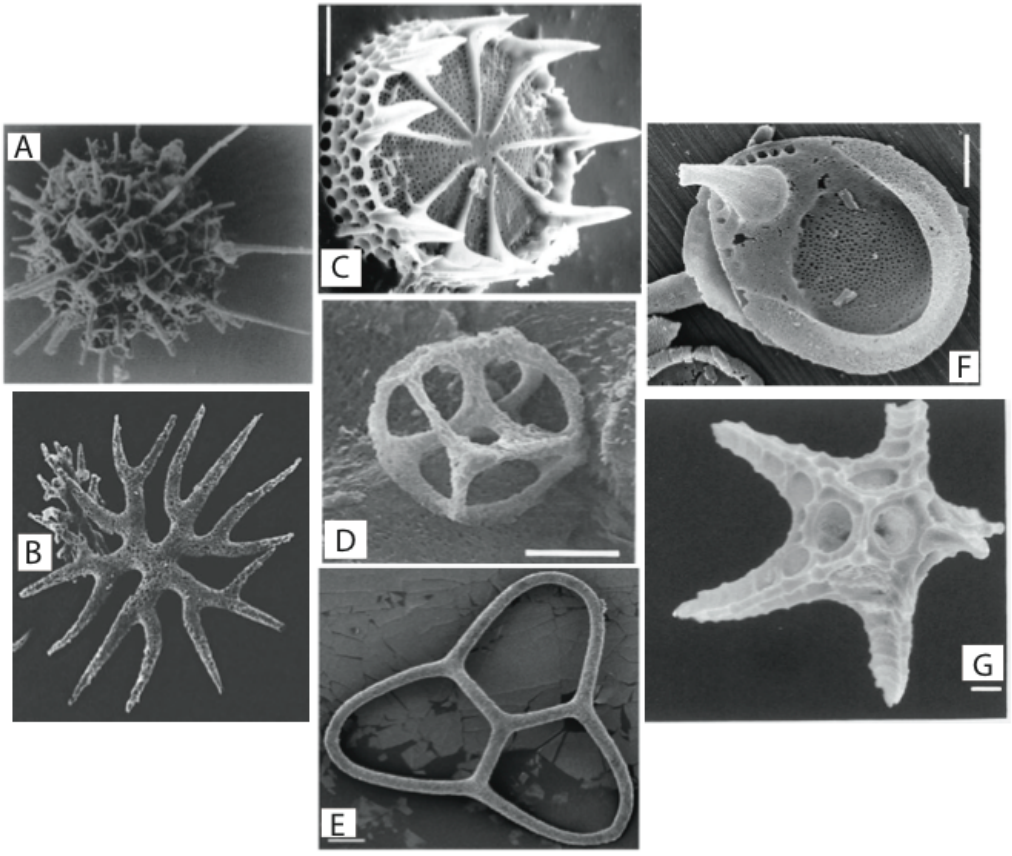

Fig. 1 A. Middle Cambrian radiolarian Georgina Basin, Queensland, Australia. Won & Below 1999
B. Early Cambrian siliceous sponge spicule Shaanxi China. Zhang & Pratt 1994
C. Lower Cretaceous diatom *Basilicostephanus ornatus* ODP Leg 113 693 (Weddell Sea) Scale bar = 5 µm. Sims et al., 2006; Gersonde & Harwood, 1990
D. Eocene ebridians *Ebrinula paradox* Southern Ocean Scale bar = 10 µm. Bohaty & Harwood 2000
E. Late Cretaceous silicoflagellate *Corbisema archangelskiana* DSDP Leg 29. McCartney et al. 2010
F. Middle Eocene chrysophytes Scale bar = 1 µm. Siver & Wolfe 2005
G. Holocene Actiniscaceae *Actiniscus pentasterias* Bering Sea, Scale bar = 5 µm. Orr & Conley 1976

A number of siliceous groups appeared in the Mesozoic, with five of the six taxa first seen in the Mesozoic having first appearances in the Cretaceous (Fig. 2**)**. Diatoms, silicoflagellates, chrysophytes, ebridians, and Actiniscaceae were first seen in the Cretaceous (Porter, in prep; Fig 1). The first appearance of diatoms is currently contested; there is strong fossil evidence for marine diatoms in the early Cretaceous (Harwood & Nikolaev, 1995; Gersonde & Harwood, 1990), yet fossil frustules have been reported from the Jurassic (Rothpletz, 1896). Rothpletz's claim cannot be verified because the samples

were lost during World War II (Falkowski, et al. 2004). Furthermore, a molecular clock estimate places the origin of diatoms at the Permian-Triassic boundary (Medlin et al., 1997; Graham & Wilcox, 2000). An early Cretaceous first appearance of diatoms is accepted here because it is based on the most reliable evidence. Actiniscaceae, a dinoflagellate with a siliceous endoskeleton, has a poor fossil record and therefore its first appearance is not as reliable as those organisms with a robust fossil record. Silicoflagellates, chrysophytes, and ebridians all have a good fossil record and there is a high degree of confidence in a Cretaceous origin for each of these groups.

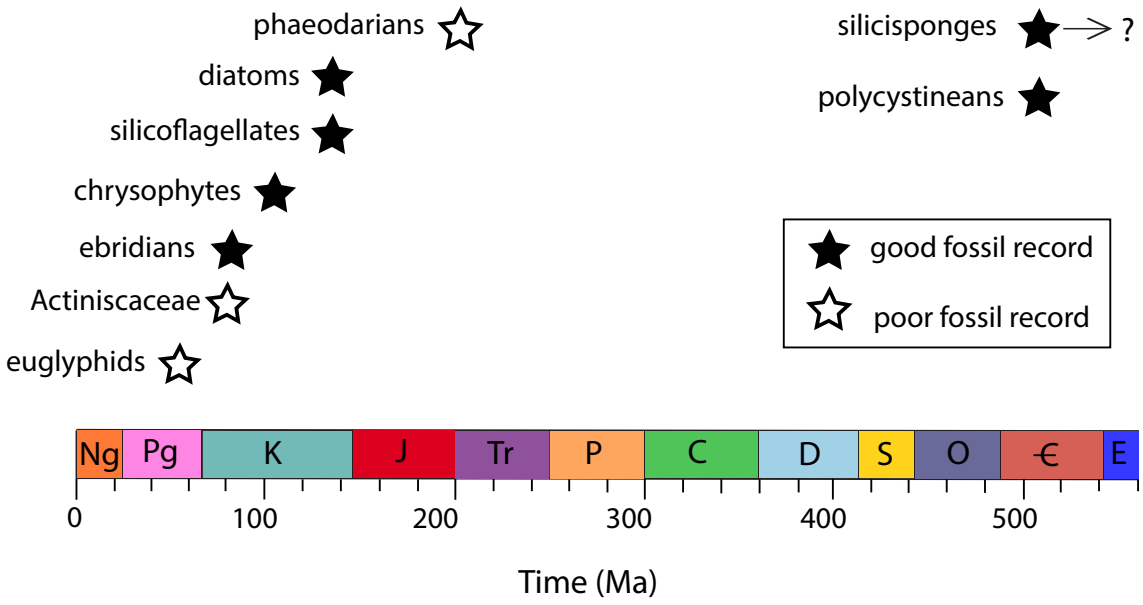

Fig. 2 The first appearances of all siliceous taxa in the Phanerozoic fossil record (Porter, in prep).

Euglyphids first appeared in the Paleogene and phaeodarians are first seen in the Triassic. Both of these groups have a poor fossil record, and like Actiniscaceae, the confidence in their time of origin based upon first appearances in the fossil record is not as high as taxa with a robust fossil record.

It is currently unknown if there is a reason why several taxa independently acquired a siliceous skeleton during the Cretaceous. It is hypothesized this was due to the influence of contemporaneous seawater chemistry. Seawater silicic acid concentrations may have been

elevated during this time, making the construction of a siliceous skeleton favorable due to the abundance of bioavailable silica. This hypothesis is based upon the following four lines of evidence.

First, evidence for calcareous biomineralizers adopting the calcium carbonate polymorph (aragonite or calcite) of contemporaneous seawater through time has been documented (Porter, 2007; 2010), indicating that seawater chemistry influences the mineralogy an organism adopts for skeletal construction.

Second, extensive evidence indicates bioavailable silica concentrations influence the growth and reproduction of siliceous taxa. When seawater silica is low, diatoms cease to reproduce (Brzezenski et al., 1990) and radiolarian skeletal robustness decreases (Harper & Knoll, 1975; Lazarus et al., 2009). In addition, sponge spicule morphology in some species is controlled by silica concentrations (Maldonado et al., 1999).

Third, radiolarians radiated at the family level during the Cretaceous (Casey et al., 1983). This event may have been influenced by an increase in the nutrient silica, for evidence exists linking increased nutrient availability to higher origination rates in the marine environment at the genus level (Cárdenas & Harries, 2010).

And fourth, a global proliferation of siliceous sponges in the early Jurassic is argued to have been partly caused by an increase in silica fluxes to shelf environments from the weathering of the Central Atlantic Magmatic Province, a continental flood basalt terrain (Ritterbush et al., 2015). Ritterbush et al. show that increased delivery of silica to seawater elicits a strong response from siliceous organisms.

Each of the above examples demonstrates the influence seawater chemistry can have on skeletonized taxa. To determine whether seawater silica fluxes were heightened and may

have influenced the acquisition of a siliceous skeleton in the Cretaceous, further evidence is amassed and discussed in this thesis. First, the Phanerozoic record of chert deposits is presented to determine if this record reflects past seawater silica concentrations. Second, the modern silica cycle is discussed so the sources and sinks of silica that operate today may inform us about silica cycles of the past. An emphasis is placed on riverine and hydrothermal inputs because they are major contributors of silica today and their inputs of silica to seawater for the geologic past may be approximated, if some reasonable but simple assumptions are made. Finally, a search for a silica proxy that can be used for the geologic past was undertaken. Linear regression analyses on modern riverine water chemistry and hydrothermal vent fluid compositions were performed. Regression analyses on global riverine data and for smaller catchments draining predominantly mafic or silicic terrains (basalt or granite) were performed to determine if any variables strongly correlate with riverine silica. Regression analyses were also performed on silica and strontium concentrations using three hydrothermal vent fluid datasets; two are from the East Pacific Rise and one is from the Mid Atlantic Ridge. In addition, two models that attempt to explain the $^{87}Sr/^{86}Sr$ seawater curve are explored to determine if this robust record may be used as a silica proxy.

III. The History of Seawater Silica & The Phanerozoic Chert Record

Seawater silica concentrations are thought to have been the highest during the Precambrian, with a stepwise decrease in the early Phanerozoic and during the Cenozoic due to the origin of siliceous taxa taking up dissolved silica (Siever, 1992; Maliva et al., 1989; Harper & Knoll, 1975; Racki & Cordey, 2000).

Precambrian seawater silica concentrations are argued to have been at or above

equilibrium for opal-CT and even amorphous silica, making seawater silica concentrations as high as 2.2 mM (millimolar or millimoles per liter) (Drever, 1974; Holland, 1984; Siever, 1992). The only silica sink during the Precambrian was abiotic reactions. Silica precipitated as solid phases such as cristobalite and amorphous silica or it was adsorbed onto clay minerals (Siever, 1992).

A decrease to between ~1 and 0.66 mM for the Cambrian – early Cretaceous has been proposed based upon the formation of nodular cherts by opal-CT (Siever, 1992), though a higher concentration of 1.8 mM has been proposed based on the formation of highly siliceous jasper deposits (Grenne & Slack, 2003). Siliceous taxa deplete seawater silica more than abiotic processes and the decrease in seawater silica during the early Paleozoic was due to a biotic influence on the global silica cycle with the first appearance of siliceous sponges and polycystineans (Siever, 1992; Maliva et al., 1989).

A decrease in seawater silica concentrations during the Cenozoic was due to the proliferation of diatoms and their efficient ability to uptake dissolved silica (Lazarus et al., 2009; Darley, 1969). Silica concentrations are unknown for the early Cenozoic; a decrease to below 0.17 mM occurred in the late Eocene (Racki & Cordey, 2000) when diatom diversity greatly increased (Falkowski et al., 2004).

Diatoms decreasing seawater silica is also evident from a decrease in radiolarian test weight and structural changes associated with less silica uptake per skeleton (Harper & Knoll, 1975; Lazarus et al., 2009) during the Cenozoic and the disappearance of desma-bearing siliceous sponges from reefs and other neritic environments during the Cretaceous and early Paleogene (Maldonado et al., 1999 and references therein).

Though a stepwise decrease in seawater silica concentrations has occurred from the

Precambrian to today, due to the evolution and diversification of siliceous taxa, silica fluxes to the ocean have varied through time. These changes in silica inputs through time would then likely influence the record of silica-rich deposits.

The silica cycle is viewed to be in steady-state over long timescales, where silica inputs to the ocean equal silica outputs (Treguer & De La Rocha, 2012; Steinberg, 1981). Therefore, if silica inputs increase, then this may be recorded in deposits of chert, the ocean's silica sink. A global compilation of the number of bedded chert deposits for each period of the Phanerozoic was presented by Hein & Parrish (1987). The majority of deposits are early diagenetic cherts originally composed of biogenic opal from radiolarians or diatom skeletons. The Cretaceous has the greatest number of bedded chert deposits, with 48 total (Fig. 3a, Hein & Parrish, 1987). This abundance of chert deposits indicate Cretaceous oceans may have been unusually high in dissolved silica if the silica cycle was in steady-state during this time. The Cretaceous was the longest period of the Phanerozoic, spanning 79 million years, and the great number of chert deposits may be due to the greater amount of time for deposits to form. In addition, the Cretaceous is younger than many of the periods of the Phanerozoic and therefore less time has passed than earlier periods to erode these chert deposits.

To determine if the number of chert deposits for the Cretaceous was much higher than the other periods of the Phanerozoic, the data from Hein & Parrish (1987) (Fig. 3a) was normalized (Fig. 3b). This was done by dividing the number of chert deposits in a period by the number of years in that period.

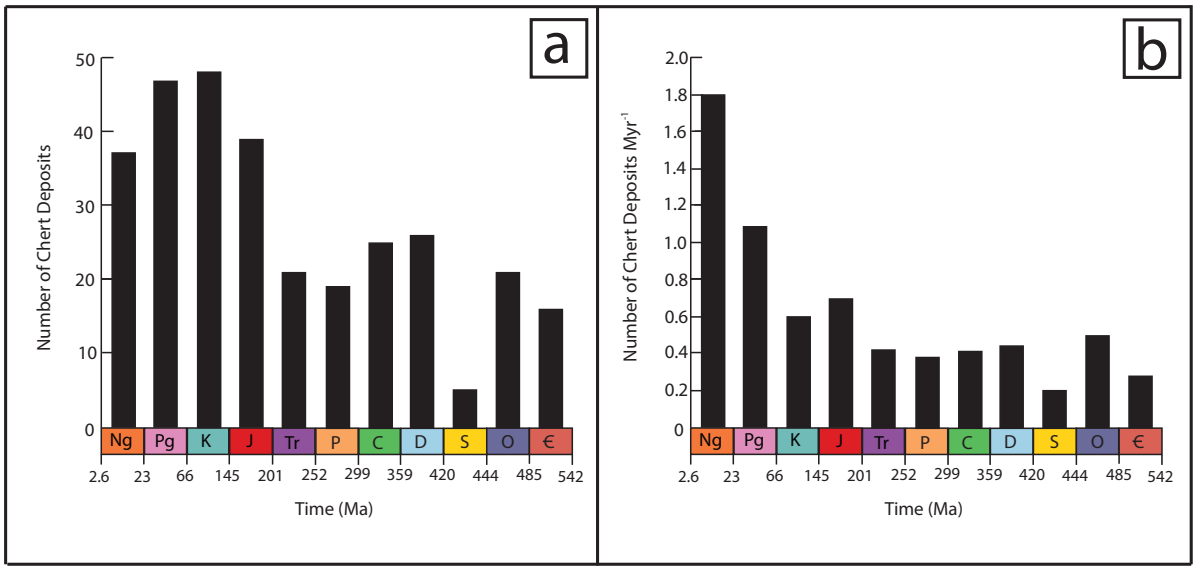

Fig. 3 a) A global compilation of the number of bedded chert deposits for each period of the Phanerozoic. b) Normalized chert deposits for the Phanerozoic. Hein & Parrish, 1987.

If the number of chert deposits in each period were a result of the effects of weathering and erosion through time, then one would expect that the number of deposits per million year would steadily decrease with age. The Neogene and the Paleogene fit this expectation, yet several older periods had higher rates of chert deposition than younger periods. For example, the Ordovician had higher rates of chert deposition than all of the following periods through the Triassic, the Devonian had higher rates than the following three periods, and the Jurassic had higher rates than the Cretaceous (0.7^{th} of a deposit Myr^{-1} and 0.6^{th} of a deposit Myr^{-1}, respectively) (Fig. 3b). Based upon the results of the normalized chert deposits, the Jurassic had the highest rate of chert deposition for the Mesozoic. This may have been due to the proliferation of siliceous sponges in the early Jurassic caused by increased silica fluxes to seawater from the weathering of the Central Atlantic Magmatic Province (CAMP) (Ritterbush et al., 2015).

Chert volumes provide a better indication of chert deposition than the number of chert deposits for a given time period, as provided in Hein & Parrish (1987). Ronov (1981)

provided chert volumes, though data for many periods of the Phanerozoic are missing because siliceous sediments were not present on the lithologic maps Ronov used to measure volumes of rock types throughout the Phanerozoic. Values for the Miocene through the early Cretaceous (minus the Oligocene), the late Triassic, the early Permian, Silurian, Ordovician, and the early Cretaceous are available. Of the available data, the early Cretaceous and the late Cretaceous have the highest volumes of siliceous deposits with 2.7×10^6 km^3 and 2.5×10^6 km^3, respectively. The Ordovician shows the next highest volume, with 1.4×10^6 km^3 of siliceous deposits. A more complete dataset on the volumes of siliceous deposits for the Phanerozoic is required to determine if the Cretaceous was a period of high chert deposition.

A factor that can influence chert deposition other than enhanced silica input to the ocean is the carbonate compensation depth (CCD). The CCD is the depth at which carbonate dissolves at the same rate it is supplied (Van Andel, 1975). The CCD has varied through time and chert deposition is greater when the CCD is shallow. This is because siliceous sedimentation is not diluted by carbonate. The majority of carbonates are deposited on continental shelves and the available silica is released to the deeper ocean (Berger & Winterer, 1974; Steinberg, 1981). The CCD was shallow, being above 4000 m during the late Jurassic through the early Cenozoic (Van Andel, 1975; Rigo et al., 2007) and this may have influenced the abundance of chert deposits during this time. The input of silica to the oceans would not have to be unusually high, though the hypothesis that both heightened silica fluxes and a shallow CCD were operating in the Cretaceous cannot be discounted.

The record of chert deposits for the Phanerozoic does not give a clear indication whether Cretaceous seas were unusually high in dissolved silica. In a further attempt to address this question, the sources of silica of the modern marine cycle are explored. The

operation of these sources are then explored for the Cretaceous.

IV. The Marine Silica Cycle

There are five sources that deliver significant quantities of silica to the ocean today. Rivers deliver the greatest amount of silica to seawater, with a dissolved inorganic load of 6.2 ± 1.8 Tmol $year^{-1}$ and a dissolved biogenic load of 1.1 ± 0.2 Tmol $year^{-1}$. The second greatest source is seafloor weathering, delivering 1.9 ± 0.7 Tmol $year^{-1}$, followed by groundwater (0.6 ± 0.6 Tmol $year^{-1}$), hydrothermal (high and low temperature, 0.6 ± 0.4 Tmol $year^{-1}$), and aeolian dust (0.5 ± 0.5 Tmol $year^{-1}$) (Treguer & De La Rocha, 2012).

The largest silica sink today is the burial of biogenic silica in marine sediments. Most silica is buried in coastal and continental margins ($3.3. \pm 2.1$ Tmol $year^{-1}$), followed by the Southern Ocean basin (2 ± 1.2 Tmol $year^{-1}$), and the open ocean (<1.04 Tmol $year^{-1}$) (Treguer & De La Rocha, 2012).

The silica inputs from rivers and hydrothermal sources may be constrained approximately for the geologic past; groundwater, aeolian dust, and seafloor weathering are far more difficult to constrain. The factors influencing riverine dissolved silica fluxes and hydrothermal silica fluxes are discussed. These topics are then extended to the Cretaceous to determine if seawater silica was heightened during this period. In addition, the widespread emplacement of ocean basin flood basalt provinces during the Cretaceous is discussed as a possible source of silica to seawater.

A. Factors that Control Riverine Input

1. Lithology

The greatest source of dissolved silica (DSi) today is from riverine input via continental weathering (Treguer & De La Rocha, 2012). Lithology, climate (temperature

and rainfall), and vegetative cover are all factors that control rates of weathering and hence the release of silica to seawater (Berner & Berner, 2012).

The lithology of a drainage basin is a major factor controlling the DSi of a river. This is not only because the silica content varies in minerals, but more importantly due to the weathering style silicate minerals undergo. Congruent weathering (the dissolution of a primary mineral without re-precipitation of a secondary mineral) releases a greater amount of silica to solution than minerals that undergo incongruent weathering and is confined to the silicate minerals olivine, amphibole, and pyroxene (Berner & Berner, 2012). Igneous rocks, namely intermediate plutonics and volcanics, yield the greatest amount of DSi for a given runoff because these rocks contain an abundance of these easily weathered minerals (Jansen et al., 2010). In addition, volcanics release an abundance of DSi because they contain volcanic glass, which weathers more rapidly than any silicate mineral. The porosity of volcanics also increases weathering rates by allowing a greater amount of surface area contact between the minerals and water (Berner & Berner, 2012).

2. Climate

Climate, namely temperature and rainfall, has also been shown to influence riverine silica fluxes. Many studies have found a positive correlation between temperature and riverine DSi release (Brady & Carroll, 1994; White & Blum, 1995; White et al., 1999; Brady et al., 1999; Dessert et al., 2003; Oliva et al., 2003). These studies were either lab experiments or on rivers draining a single lithology. A positive correlation between temperature and DSi yield has not been identified for rivers draining a variety of lithologies. The effect of temperature on riverine DSi is likely due to the differences in silicate weathering products that form in different climate zones. For example, in tropical climates

silicate minerals typically weather to kaolinite, which releases 1.5 times as much DSi as the weathering product smectite seen in temperate climates (Meybeck, 1980).

Rainfall is another factor influencing DSi yield. Higher rainfall in a region typically translates to higher river runoff, which in turn leads to greater DSi yields (Bluth & Kump, 1994; Hartmann et al., 2010; White & Blum, 1995). Runoff has been identified as the most important factor for predicting riverine DSi based on a model calibrated to river chemistry data from 142 monitoring stations in the conterminous USA (Jansen et al., 2010). Like temperature, a wetter climate is associated with higher riverine DSi due to weathering product formation. For example, in a dry climate albite plagioclase weathers to the clay smectite, yet in a wetter climate with higher runoff, albite weathers to the clay mineral kaolinite, which releases all of the silica to solution instead of only two-thirds as smectite does (Berner & Berner, 2012).

3. Vegetative Cover

Lastly, vegetative cover influences riverine DSi fluxes by enhancing weathering rates, acting as a direct source of silica, and sequestering silica on land. Plants increase weathering rates by secreting organic acids that accelerate the rate of mineral dissolution, they recirculate water via evapotranspiration, and fracture rocks with their roots, which increases the surface area for water-mineral interaction (Berner & Berner, 2004). Studies have shown that lichens and trees increase basalt weathering rates compared to non-vegetated river basins (Brady et al., 1999; Moulton et al., 2000). Furthermore, many plants contain amorphous silica bodies called phytoliths that provide structural support. These readily dissolve and increase riverine silica (Alexandre et al., 1997). DSi from phytolith dissolution is twice that of DSi from silicate weathering and cycling of silica in terrestrial

ecosystems should be taken into account when attempting to track DSi from silicate weathering (Alexandre et al., 1997). Plants can also keep silica from reaching the ocean. In terrestrial forested ecosystems, silica can be sequestered in plants where it becomes a part of the terrestrial silica cycle, decreasing the amount of silica that reaches the ocean (Conley, 2002). The assemblage of plants in an ecosystem largely controls how much silica is sequestered. For example, angiosperms typically have a greater silica requirement than gymnosperms and angiosperms would therefore decrease seawater silica delivery to a greater extent (Conley & Carey, 2015; Hodson et al., 2005).

The above factors do not act alone in controlling riverine DSi, but they instead display a synergistic effect. Other factors have been identified that influence weathering rates and hence DSi release, yet they are accepted to have a lesser influence on riverine DSi than the factors identified here (Jansen et al., 2010; Brady & Carroll, 1994; White & Blum, 1995; White et al., 1999; Brady et al., 1999; Dessert et al., 2003; Oliva et al., 2003; Bluth & Kump, 1994; Hartmann et al., 2009; Berner & Berner, 2012) and are therefore beyond the scope of this study. The factors that influence riverine DSi today when applied to the geologic past have great potential to elucidate what riverine silica fluxes to seawater may have been like and are the next topic of discussion.

B. Factors that Control Riverine Input Operating in the Cretaceous

1. Continental Weathering in the Cretaceous

Lithology may have played an important role in silica delivery to Cretaceous oceans, yet this is difficult to determine due to the effects of weathering and erosion on bedrock through time. Because volcanics weather rapidly and release an abundance of DSi, this rock type would have the greatest potential for increasing seawater silica delivery from land to

ocean if an abundance of continental basalt was emplaced during the Cretaceous. A study of the weathering of the Central Atlantic Magmatic Province (CAMP), a continental flood basalt that was emplaced 205 – 191 Ma (Bryan & Ernst, 2008), indicates the silica input to Jurassic seas was great and caused a global proliferation in siliceous sponges (Ritterbush et al., 2015). No continental flood basalts were emplaced during the Cretaceous, except for the Deccan Traps at the close of the period, though many voluminous ocean basin flood basalt provinces were emplaced. One silicic large igneous province, the Whitsunday, was emplaced 132 – 95 Ma, with the majority of emplacement occurring between 118 – 113 Ma and at 110 – 105 Ma (Bryan & Ernst, 2008). The CAMP may have been the largest continental flood basalt of the Phanerozoic, originally covering an estimated 1.12×10^7 km^2 (McHone, 2003) and was likely much greater than the Whitsunday, with a preserved area of 3×10^6 km^2 (Bryan, 2005). Silica liberated from the CAMP would likely have been greater than that from the Whitsunday, yet an estimate for the original aerial extent of the Whitsunday and research on the amount of Si liberated from the dominant rock lithology of each LIP would provide a more accurate assessment.

2. Climate During the Cretaceous

The climate during the Cretaceous may have increased silica delivery from the continents to the ocean. Evidence suggests the mid–late Cretaceous was very warm, reaching maximum sea surface temperatures 3-5 ^oC warmer than today with unusually warm polar temperatures (Wilson & Norris, 2001). Paleoclimate and paleobotanical data indicate the Arctic Ocean was very warm at the end of the Cretaceous (Herman & Spicer, 1997; Herman & Spicer, 1996). In addition, the Cretaceous is thought to have been exceptionally humid (Tardy et al., 1989). The effects of continental size and their latitude influenced the

global water cycle during the Cretaceous, causing this period to have the highest global continental runoff of the past 400 million years (Tardy et al., 1989; Fig. 4). Global runoff reached 52 x 10^6 km^3/My during the upper Cretaceous and was far greater than the global runoff of 39.7 x 10^6 km^3/My seen today (Tardy et al., 1989). This increase in rainfall was attributed to the separation of continents and the great amount of landmass at equatorial and temperate latitudes (Tardy et al., 1989). This increase in rainfall would have increased runoff, leading to an increase in DSi delivery to seawater.

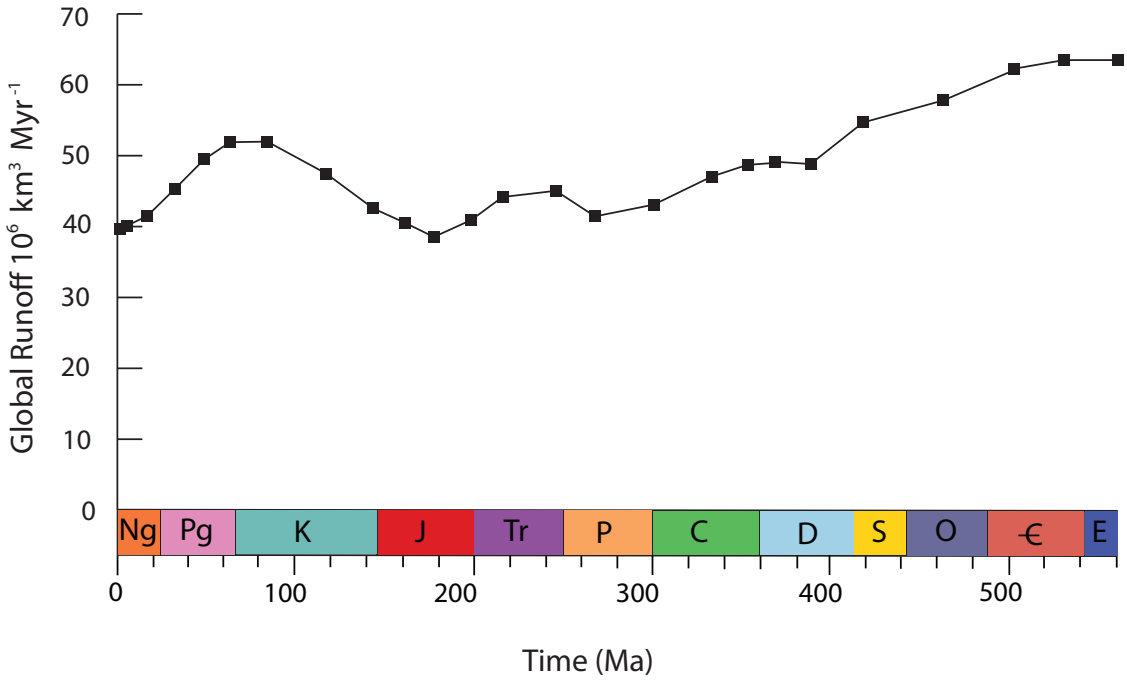

Fig. 4 The calculated global continental runoff for the past 560 million years. Modified from Tardy et al. 1989.

3. Cretaceous Vegetative Cover

The vegetation on land during the Cretaceous also may have played a role in the marine silica cycle. Silica uptake has occurred in terrestrial plants since their origins over 400 million years ago (Trembath-Reichert et al., 2015). Early land plants such as lycophytes, horsetails, and early ferns in the middle and late Paleozoic contained high amounts of silica. Conifers, which contain a lower amount of silica than these early land plants, radiated

during the Mesozoic and silica-rich grasses came to dominate during the Cenozoic (Trembath-Reichert, 2015 and references therein). Plants that contain high amounts of silica sequester a greater amount of silica on land than vegetation with low silica requirements. The Triassic and the Jurassic may have been a time when less silica was sequestered on land due to the radiation of silica-poor gymnosperms, yet the rapid radiation of angiosperms in the early Cretaceous (Moore et al., 2007) likely decreased the flux of silica from the continents to the ocean. In addition, the Paleozoic and the Cenozoic were likely times of high silica sequestration on land (Conley & Carey, 2015) because high-silica-containing lycophytes and early-diverging ferns dominated the Paleozoic terrestrial landscape, (Trembath-Reichert et al., 2015) and grasses with high silica requirements diversified in the Cenozoic (Falkowski et al., 2004).

The warm and wet climate during the Cretaceous, especially during the mid–late Cretaceous, could have accelerated continental weathering, heightening silica delivery to seawater. The radiation of angiosperms during the Cretaceous may have sequestered a significant amount of silica on land, keeping it from reaching the ocean. Furthermore, it is difficult to assess the lithological composition of the continents during the Cretaceous and whether this factor influenced seawater silica in a great way. Yet, there is no evidence for the widespread emplacement of continental flood basalts during this period, except for the Deccan traps emplaced at the Cretaceous – Paleogene boundary. Research on the potential silica release from the Whitsunday, a silicic large igneous province, emplaced during the mid Cretaceous, would be fruitful.

C. Hydrothermal Input

Hydrothermal silica comes from both a high temperature (350 ^{o}C ± 30 ^{o}C) axial

source along mid-ocean ridges and a low temperature (< 75 ^{o}C) off-axial, diffuse ridge flank source (Treguer & De La Rocha, 2012). Hydrothermal vents along mid-ocean ridges have a higher flux of silica than ridge flank sources. This is because more silica is leached from the ocean crust at high temperatures, whereas at ridge flanks, cooling occurs and some silica is removed via secondary mineral formation on the seafloor (Wheat & McManus, 2005).

The flux of silica from hydrothermal sources is an order of magnitude lower than that of riverine sources today (Treguer & De La Rocha, 2012; Table 1), yet the concentration of silica in hydrothermal fluids is far greater than that of river water. The discharge weighted average dissolved silica concentration of riverine water is 158µM, (Dürr et al., 2011) whereas the average silica concentration in hydrothermal fluids taken from seven vent sites worldwide is ~17.5 mM (Von Damm, 1990), about 100 times as large as riverine silica concentrations. Though the flux of rivers is far greater than that of the hydrothermal flux today, the flux of each has likely varied throughout geologic history.

Component	Flux (Tmol Si year^{-1})
Rivers, dissolved silica	6.2 ± 1.8
Rivers, biogenic silica	1.1 ± 0.2
Seafloor weathering	1.9 ± 0.7
Groundwater	0.6 ± 0.6
Hydrothermal (high and low temperature)	0.6 ± 0.4
Atmosphere (aeolian)	0.5 ± 0.5

Table 1. Annual flux of silica from significant sources to the modern ocean. Treguer & De La Rocha, 2012.

One factor that may be responsible for changes in hydrothermal silica fluxes are spreading rates. A greater amount of hydrothermal activity occurs along faster spreading ridges than slower spreading ridges. This is evidenced by the inert isotope ^{3}He used to track hydrothermal activity. Larger ^{3}He plumes emanate from faster spreading ridges than slower

spreading ridges and in the South Atlantic ^{3}He concentrations are an order of magnitude below those of the Pacific. This great difference has been attributed to the slower spreading rates of the South Atlantic and the faster rates of the Pacific (Devey et al., 2010; Lupton, 1998; Rüth et al., 2000; Lupton et al., 2004). Greater hydrothermal fluxes come from fast spreading ridges and therefore greater silica fluxes would likely come from fast spreading ridges as well.

Seafloor spreading rates and mid-ocean ridge lengths are thought to have been greater during the Cretaceous than today (Coltice et al., 2013; Müller et al., 2008; Gaffin, 1987). Seafloor spreading rates increased significantly in the early–mid Cretaceous of the Panthalassic ocean based on magnetic lineations in the Pacific (Larson & Chase, 1972; Nakanshi & Winterer, 1998; Seton et al., 2009). In addition, Cretaceous mid-ocean ridge lengths were longer due to the break up of Pangea and formation of the Pacific plate (Larson, 1991; Coltice et al., 2013). These two factors led to very high rates in seafloor production during the Cretaceous (Fig. 5).

Three studies have independently concluded seafloor production was heightened during the Cretaceous. Müller et al. (2008) created tectonic plate reconstructions for the past 140 Ma and used seafloor area-age data to construct a crustal production curve. Coltice et al. (2013) used plate reconstructions from Seton et al. (2012) to determine seafloor spreading rates for the past 250 Ma. These reconstructions were created using >70,000 magnetic anomalies and fracture zone identifications for preserved seafloor crust. For subducted crust the assumptions of symmetry at spreading zones was used to reconstruct oceanic crust (Müller et al., 2008; Seton et al., 2012). Lastly, Gaffin (1987) created a seafloor production curve for the past 550 Ma by inverting the sea level curve of Vail et al. (1977). This method

relies on the assumption that long-term sea level changes are due to variations in the volumetric rate of oceanic crust production.

The three curves broadly agree, creating a concave down shape with the highest rates of seafloor production during the Cretaceous. The average seafloor production for the Cretaceous was 4.53 $km^2\ yr^{-1}$, whereas the Jurassic had rates of 3.35 $km^2\ yr^{-1}$ and the post Cretaceous had rates of 3.27 $km^2\ yr^{-1}$. There are uncertainties in the rates of seafloor production over the past 200 Ma, evidenced by several times where the three curves do not agree. The largest discrepancy is in the early Cretaceous between 150 – 130 Ma, with the curve of Coltice et al. reaching 1.5 times the seafloor production of Gaffin (1987) at 145 Ma (Fig. 5). All three curves agree quite well from 0 – 30 Ma and 120 – 130 Ma and two curves (Gaffin 1987 & Coltice et al. 2013) agree well from 170 – 180 Ma, a time for which the Müller et al. (2008) curve lacks data. The three curves do agree on a very gross scale for the rest of the time plotted, the production rates are higher during the Cretaceous than before or after this period, yet upon closer inspection, there are disagreements in production rates for the for the rest of the time plotted. An average of the three crustal production curves was calculated and shows seafloor production rates peaked at 5.1 $km^2\ year^{-1}$ at 120 Ma (Fig. 5), which is approximately 1.8 times greater than seafloor production rates today.

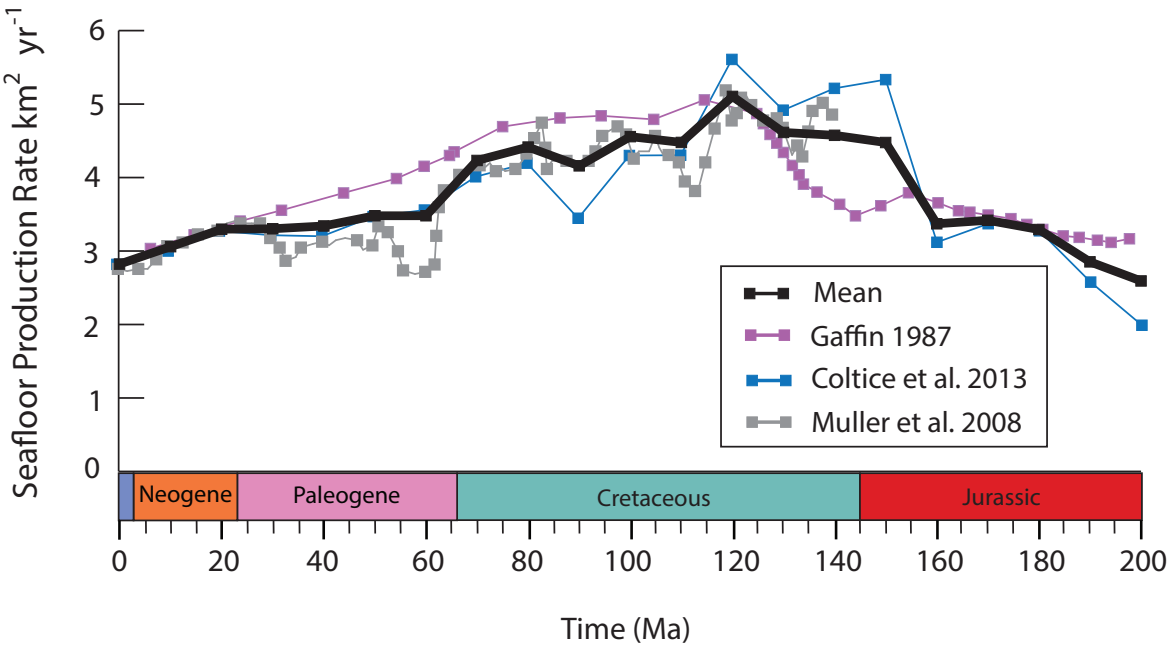

Fig. 5 Seafloor production rates for the past 200 Ma. Three independently derived curves (Gaffin, 1987; Coltice et al., 2013; Müller et al., 2008) and an average of these three curves are shown.

The increased spreading rates during the Cretaceous would have led to increased hydrothermal activity and likely an increase in silica to seawater from this heightened hydrothermal activity. Further evidence from the seawater $\delta^{34}S$ record indicates increased hydrothermal activity was characteristic of the Cretaceous, especially from 120 – 100 Ma (Paytan et al., 2004). Seafloor production rates during the Cretaceous were approximately 35% greater than those of the Jurassic and approximately 38% greater than those of the post-Cretaceous based on the mean seafloor production rate curve shown in Fig. 5. Though exactly how much more silica would have been released to seawater from this amount of change in seafloor production is currently unknown.

In addition to increased seafloor production at mid ocean ridges, many voluminous ocean basin flood basalt provinces were emplaced during the Cretaceous (Fig. 6). These ocean basin flood basalt provinces have been linked to a decrease in the heat flux emanating from the core that led to a forty-two million year span without geomagnetic reversals known

as the Cretaceous Normal Polarity Superchron (125 – 83 Ma; Olson & Amit, 2015) An oceanic basin flood basalt province is a type of large igneous province, defined as a magmatic province with an areal extent exceeding 0.1 million km^2, an igneous volume greater than 0.1 million km^3, and a maximum lifespan of ~50 million years. They have igneous pulses that are short lived (~1 – 5 million years) in which a majority (>75%) of the total volume is emplaced (Bryan & Ernst, 2008). Each of the three seafloor production curves in Fig. 5 incorporated the emplacement of ocean basin flood basalt provinces in addition to oceanic crust that is produced along mid-ocean ridges. Therefore, Fig. 5 shows the production rate of all seafloor volcanics for the past 200 Ma. The emplacement of these voluminous ocean basin flood basalt provinces was unique to the Cretaceous based on the 200 million year old seafloor record and these events are explored as a possible source of silica to seawater.

The volumes and ages of all large igneous provinces (LIP) for the past 200 million years were used to calculate global LIP emplacement rates. These data were then graphed against total seafloor production rates to determine if the LIP rates were substantial on a global level (Fig. 6). Because all seafloor production rate curves in Fig. 5 include ocean basin flood basalt provinces, the comparison between seafloor production rate data and the production rate of ocean basin flood basalt provinces in Fig. 6 is not completely accurate, yet the comparison still provides a fair assessment of how large the ocean basin flood basalt provinces were compared to global seafloor production at mid-ocean ridges. Fig. 6 may aid in determining how much silica was released from ocean basin flood basalt provinces. If production rates influence silica release on the seafloor, then comparing ocean basin flood basalt province production rates to those of background mid-oceanic ridge basalt (MORB)

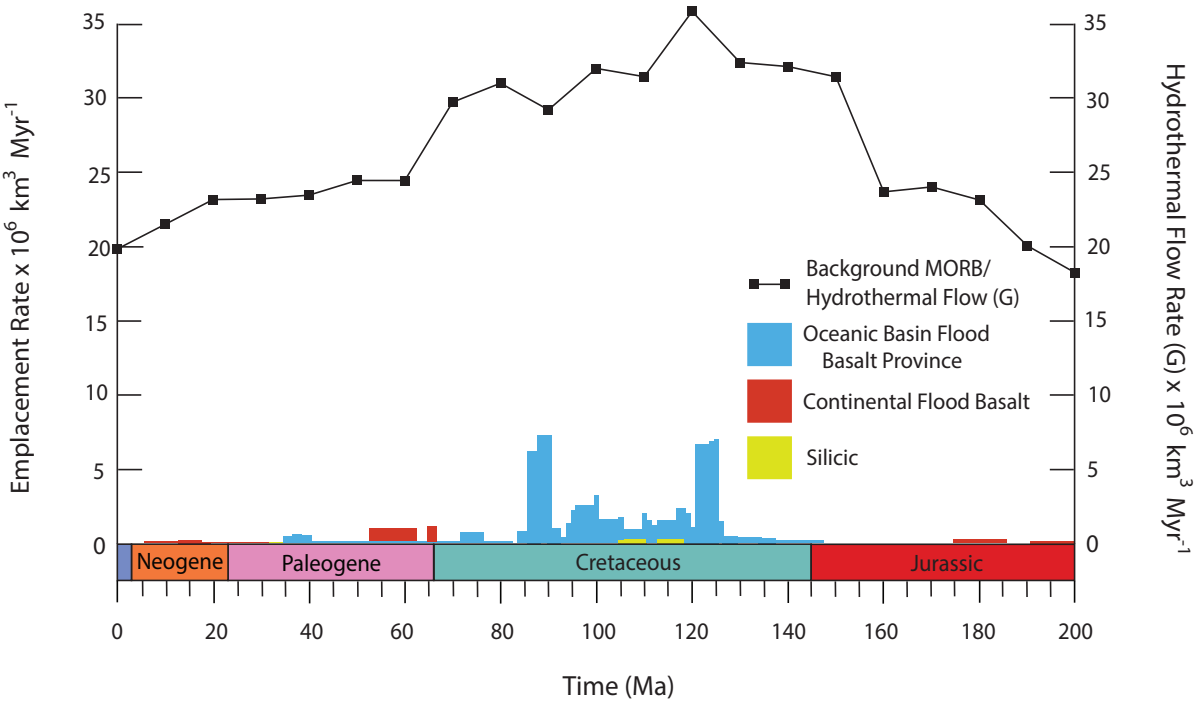

Fig. 6 Emplacement rates for the mean seafloor production curve and the hydrothermal flow rates for the past 200 Ma (black line). Emplacement rates of twenty-six large igneous provinces (ocean basin flood basalt provinces, continental flood basalts, and silicic) for the past 200 Ma

would provide the relative amount of silica released from ocean basin flood basalt provinces.

The emplacement rates of LIPs were determined by compiling from the literature the total volume and total duration (the difference between the youngest and oldest age) for all LIPs emplaced within the past 200 Ma. The types of LIPs include ocean basin flood basalt provinces, continental floods basalts, and silicic large igneous provinces. The last two types of LIPs were plotted for completeness and to identify whether any voluminous silicic or continental flood basalt LIPs were emplaced during the Cretaceous that may have acted as a significant source of silica. Emplacement rates were then calculated in Excel for each LIP by dividing the total volume in 10^6 km^3 by the total duration in millions of years (Table 2).

In addition, for those LIPs with available data on pronounced magmatic pulses in which a substantial amount of the LIP was emplaced within a relatively brief time compared to total duration, emplacement rates for the pulses were calculated when information on the

estimated percentage of total volume emplaced during the pulse(s) were available. The volume emplaced during the pulse(s) were then divided by the total duration of the pulse(s) in millions of years. When the percentage of the total LIP volume emplaced during the pulse(s) was unknown, the total volume was divided by the duration of the pulse(s).

Forty-one large igneous provinces emplaced during the past 200 Ma were found in the literature. Twenty-six of these had total volumes and total durations available. Eruptive fluxes were calculated for each of these and subsequently graphed. Six of the LIPs were continental flood basalts, three were silicic large igneous provinces, and seventeen were ocean basin flood basalt provinces. Total volumes, duration, and calculated eruptive fluxes are shown below (Table 2). The remaining fifteen large igneous provinces were excluded from the calculations due to a lack of total duration, unknown volumes, or total volume was determined to be too small (Table 3).

The rate of the volume of oceanic crust emplaced for the past 200 Ma was created by multiplying the average seafloor production curve (from Fig. 5) by 7 km, the thickness of the oceanic crust.

The emplacement rates of ocean basin flood basalt provinces are relatively small compared to the total seafloor production rates for most of the past 200 Ma (Fig. 6), yet there are two times when ocean basin flood basalt province emplacement rates were especially pronounced. From 88 – 90 Ma emplacement rates were 7.24 x 10^6 km^3 Myr^{-1}, and from 121 – 124 Ma, rates were 6.63 x 10^6 km^3 Myr^{-1} from 121 – 123 and at 124 Ma were 6.82 x 10^6 km^3 Myr^1. These rates were still smaller than the global mid-ocean ridge (MORB) production rates, yet ocean basin flood basalt provinces represented approximately 25% and 18% of total seafloor volcanic production from 88 - 90 and 121 –124, respectively,

which is a fairly significant amount of oceanic crust that was *not* produced at mid-ocean ridges. The high seafloor production rates at around 85 – 90 Ma and 120 – 125 Ma are also times when ocean basin flood basalt province production rates were high (Fig. 6). Because ocean basin flood basalt provinces were accounted for in the seafloor production rate curves of Coltice et al. (2013), Müller et al. (2008), and Gaffin (1987), this temporal alignment in high production rates places confidence in the seafloor production rate curve. In addition, the production rates of ocean basin flood basalt provinces compared to those of background MORB would be slightly higher than the 25% and 18% previously cited because the LIPs were incorporated into each of the three seafloor production rate curves.

The comparison of ocean basin flood basalt province emplacement rates with those of mid-ocean ridge production as a means for elucidating silica from ocean basin flood basalt provinces is contingent upon the assumption that the mechanism for silica release is the same or similar for each. To date, no evidence exists for hydrothermal vents associated with ocean basin flood basalt provinces and indeed it has been argued that they do not have shallow enough chambers to support hydrothermal vents (Jones et al., 1994). This does not preclude ocean basin flood basalt provinces from releasing significant quantities of silica to seawater. The silica released from ocean basin flood basalt provinces may have been diffusive, as is silica release at mid ocean ridge flanks (Treguer & De La Rocha, 2012) or there may have been eruptions on the seafloor that released silica to seawater. Currently this is speculative; further research on ocean basin flood basalt province emplacement is required to elucidate silica release from LIPs. If emplacement rates of ocean basin flood basalt provinces are linked to silica release, then the greatest amount of silica input would have occurred from 88 – 90 Ma and 121 – 124 Ma when emplacement rates were the highest.

Name	Type of LIP	Total Volume (x 10^6 km^3)	Total Duration (Ma)	Calculated non-pulse flux (x 10^6 km^3 Myr^{-1})	Pulse Volume Used	Pulse Duration (Ma)	Calculated Pulse Flux (x 10^6 km^3 Myr^{-1})	References
Columbia Flood Basalts	CFB	1.3	17 - 6	0.12	95% of total volume = 1.23	16.6 - 15.3	0.95	Bryan & Ernst 2008; Eldholm & Coffin 2000; Courtillot & Renne 2003
Afro - Arabia	CFB	1.2	31 - 14	0.07	80% of total volume = 0.96	31 - 29.5	0.64	Bryan & Ernst 2008; Courtillot & Renne 2003; Rochette et al. 1998
Sierra Made Occidental	Silicic	0.39	38 - 20	0.02	100% (0.39)	38 - 28; 24 - 20	0.05	Bryan & Ernst 2008
Northern Kerguelen	OP	2.3	40 - 35	0.46	——	——	——	Coffin et al. 2002
Northern Atlantic	CFB	8	62 - 53	0.89	100% (8)	62 - 58; 56 - 53	1.14	Bryan & Ernst 2008
Deccan Traps	CFB	1.2	67 - 63	0.3	90% = 1.08	66 - 65	1.08	Sen & Chandrasekharam 2011; Owen-Smith et al. 2013
Ninetyeast Ridge	OP	4.7	82 - 37	0.1	——	——	——	Coffin et al. 2002
Madagascar	OP	4.4	90 - 84	0.73	——	——	——	Bryan & Ernst 2008; Eldholm & Coffin 2000
Caribbean-Colombian	OP	4.5	95 - 69	0.17	100% (4.5)	92 - 88; 76 - 72	0.56	Bryan & Ernst 2008; Eldholm & Coffin 2000
Agulhas + Maud Rise + NE Georgia Rise	OP	5.3	100 - 94	0.88	——	——	——	Parsiegla et al. 2008; Eldholm & Coffin 2000

Name	Type of LIP	Total Volume ($\times 10^6$ km^3)	Total Duration (Ma)	Calculated non-pulse flux ($\times 10^6$ km^3 Myr^{-1})	Pulse Volume Used	Pulse Duration (Ma)	Calculated Pulse Flux ($\times 10^6$ km^3 Myr^{-1})	References
Broken Ridge	OP	4.1	100 - 95	0.82	——	——	——	Coffin et al. 2002
Central Kerguelen	OP	4.5	105 - 100	0.9	——	——	——	Coffin et al. 2002
Elan Bank	OP	0.3	110 - 105	0.06	——	——	——	Coffin et al. 2002
Hess Rise	OP	9.1	111 - 88	0.4	——	——	——	Bryan & Ernst 2008; Eldholm & Coffin 2000
Hikurangi Plateau	OP	2.7	118 - 96	0.12	——	——	——	Eldholm & Coffin 2000; Hoernle et al. 2010
Southern Kerguelen	OP	8.5	119 - 110	0.94	——	——	——	Coffin et al. 2002
Manihiki	OP	8.8	126 - 117	0.98	——	——	——	Timm et al. 2011; Eldholm & Coffin 2000
Ontong Java	OP	44.4	129 - 119; 90 - 86	3.17	100% (44.4)	125 - 121; 90 - 86	5.55	Mahoney et al. 1993; Tejada et al. 1996, 2002; Eldholm & Coffin 2000
Naru Basin	OP	0.9	130 - 110	0.5	——	——	——	Bryan & Ernst 2008; Eldholm & Coffin 2000
Whitsunday	Silicic	2.5	132 - 95	0.07	——	——	——	Bryan et al. 2012; Bryan & Ernst 2008

Name		Total Volume (x 10^6 km^3)	Total Duration (Ma)	Calculated non-pulse flux (x 10^6 km^3 Myr^{-1})	Pulse Volume Used	Pulse Duration (Ma)	Calculated Pulse Flux (x 10^6 km^3 Myr^{-1})	References
Magellan Rise	OP	1.8	135 - 100	0.05	——	——	——	Bryan & Ernst 2008; Eldholm & Coffin 2000
Parana-Etendeka	OP	2.35	138 - 125	0.18	80% of 2.35 = 1.88	134 - 132	0.94	Gladczenko et al. 1997; Bryan & Ernst 2008; Gibson et al. 2006; Courtillot & Renne 2003
Shatsky Rise	OP	4.3	147 - 124	0.19	——	——	——	Sager 2005; Sager et al. 1999; Bryan & Ernst 2008
Karoo-Ferrar	CFB	2.5	184 - 174	0.25	100% (2.5)	184 - 179	0.5	Courtillot & Renne 2003; Duncan et al. 1997; Jourdan et al. 2007
Chon Aike	Silicic	0.23	188 - 153	0.01	——	——	——	Pankhurst et al. 1998; 2000; Bryan & Ernst 2008
Central Atlantic Magmatic Province	CFB	2	205 - 191	0.14	100% (2)	202 - 200	1	Marzoli et al. 1999; Bryan & Ernst 2008; Courtillot & Renne 2003

Table 2. Large igneous provinces used in the non-pulse and pulse calculations shown in Fig. 6 & 7. CFB = continental flood basaslt OP = oceanic flood basalt province

Name	Volume (x 10^6 km^3)	Age (Ma)	References
Seychelles	?	63.5 – 65	Owen-Smith et al. 2013
Sierra Leone Rise	2.5	70	Bryan & Ferrari 2013; Eldholm & Coffin 2000
Wallaby Plateau	1.2	96	Ernst & Buchan 2002
Marie Byrd Land	?	110	Ernst & Buchan 2002
Sylhet Traps	?	117	Ghatak & Basu 2011
Naturaliste Plateau	1.2	132	Eldholm & Coffin 2000; Zhu et al. 2009
High Arctic	0.05	130-80 ; 85-60	Bryan & Ernst 2008; Maher 2001
Bunbury Basalts	0.001	132 – 123	Coffin et al. 2002
Rajmahal Traps	0.03	118 – 117	Coffin et al. 2002
Skiff Bank	0.3	68	Coffin et al. 2002
Comei	?	132	Bryan & Ferrari 2013
Mozambique Ridge	?	140 – 122	Gohl et al. 2011, Ben-Avraham et al. 1995, Konig & Jokat 2010
Exmouth Plateau	?	160	Bryan & Ferrari 2013
Dronning Maud Landing	?	182	Bryan & Ferrari 2013
Tasman	?	190	Bryan & Ferrari 2013

Table 3. Large Igneous Provinces that were excluded from the calculations of emplacement rates over the past 200 Ma.

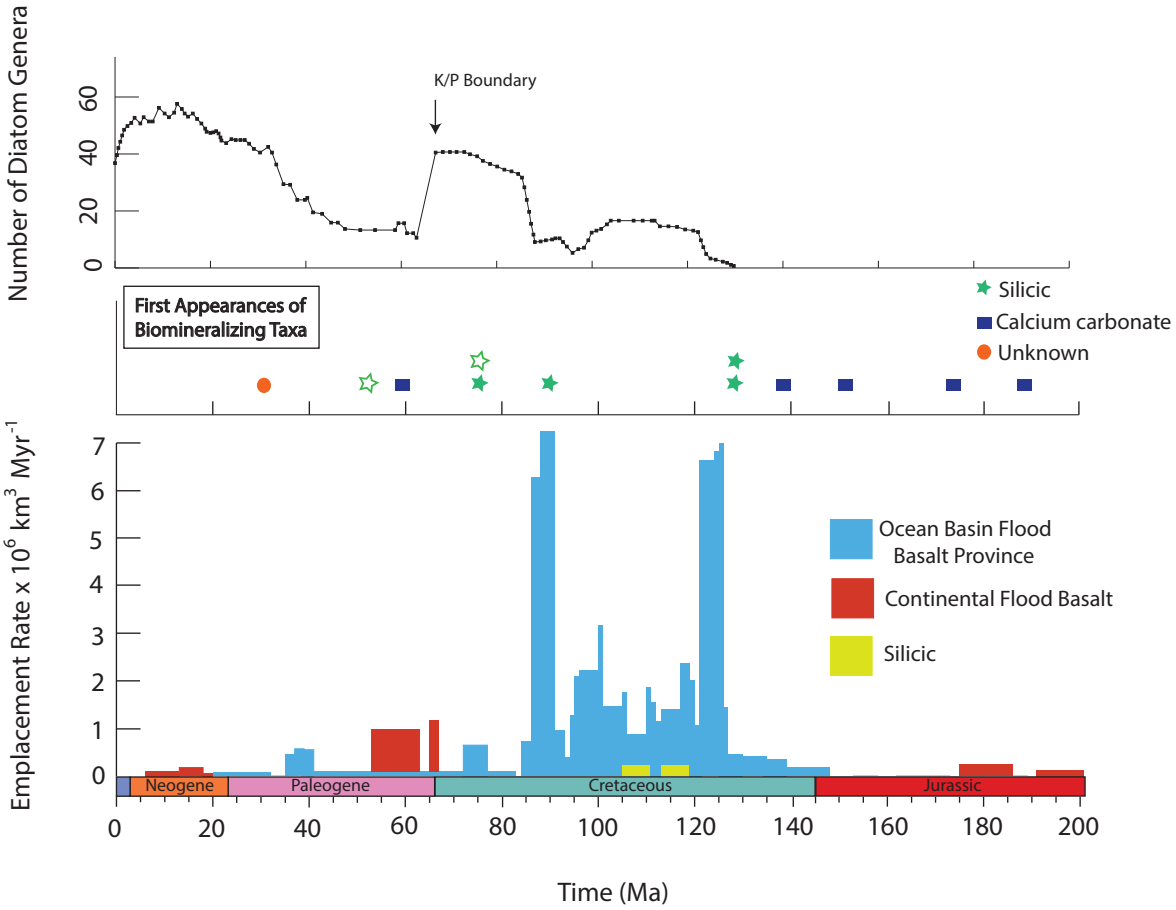

Fig. 7 Emplacement rates of twenty-six large igneous provinces, the first appearances of all skeletonized taxa (Porter, in prep), and a diatom diversity curve at the genus level (Falkowski et al., 2004) for the past 200 Ma

The emplacement rates of large igneous provinces were then graphed next to the first appearances of siliceous taxa in the fossil record and a diatom diversity curve at the genus level (Fig. 7) to determine the temporal alignment between times of high oceanic plateau emplacement and siliceous taxa. If times of high ocean basin flood basalt province emplacement coincide with times of increased diatom diversity or first appearances in the fossil record, this may have been from enhanced silica input from ocean basin flood basalt provinces.

Figure 7 was created using the LIP emplacement rate data from Table 2, a diatom diversity curve at the genus level, (taken from Falkowski et al., 2004) and the first

appearances of all biomineralizing taxa from the past 200 Ma was provided by Susannah Porter (Porter, in prep; Table 4). These organisms represent the *de novo* acquisition of silica biomineralization from non-mineralizing ancestors, representing the independent acquisition of silica mineralization.

Name	First Appearance	Skeletal Mineralogy	References
Didemnid ascidians	Early Jurassic; Upper Toarcian	Aragonite	Buge & Monniot 1972
Sabellid worms	Early Jurassic; Upper Sinemurian	Aragonite (suggestive, not convincing)	Vinn & Motus 2008
Cheilostome bryozoans	Late Jurassic	Calcite	Taylor 1994
Helioporacean octocorals	Early Cretaceous	Aragonite	Bayer 1956
Stylasterid hydrozoans	Paleocene	Aragonite	Cairns 1984
Cirratulid worms	Oligocene	Unknown	Fischer et al. 2000
Diatoms (marine)	Early Cretaceous	Silica	Sims et al. 2006
Silicoflagellates	Early Cretaceous	Silica	McCartney et al. 2010; McCartney et al. 1990
Chrysophytes	Middle Cretaceous	Silica	Data drawn from Porter (2010) and Porter (in prep)
Ebridians	Late Cretaceous	Silica	Moshkovitz et al. 1983
Actiniscaceae	Late Cretaceous	Silica	Dumitrica 1973; Rai et al. 2008
Euglyphids	Paleogene	Silica	Alves et al. 2010; Schmidt et. al. 2010

Table 4. The first appearances of all biomineralizing taxa from the past 200 Ma

Indeed, it is striking that the first appearance of chrysophytes in the middle Cretaceous occurs when there are high ocean basin flood basalt province emplacement rates (Fig. 7). In addition, the first appearances of diatoms and silicoflagellates are seen during times of heightened ocean basin flood basalt province production as well. Yet the first appearances of siliceous taxa in the late Cretaceous do not coincide with exceptionally high flood basalt production.

It is unknown if Cretaceous ocean basin flood basalt provinces acted as a significant source of seawater silica. It is striking that the emplacement of a large igneous province on land is thought to have had global effects on seawater chemistry by releasing silica from the rapid weathering of basalt (Ritterbush et al., 2015) and LIPs emplaced on the ocean floor

may have also affected global seawater silica, influencing the biomineralization of siliceous taxa. Further research is required to determine if a link exists between the ocean basin flood basalt provinces of the Cretaceous and siliceous taxa. Based upon the results of Fig. 7 this may prove to be a fruitful and exciting endeavor.

Thus far possible factors for heightened seawater silica have been discussed. The warm, wet climate (Wilson & Norris, 2001; Tardy et al., 1989) characteristic of the Cretaceous may have enhanced riverine silica fluxes to the ocean and the increased mid-ocean ridge lengths, fast seafloor spreading rates, and the emplacement of voluminous ocean basin flood basalt provinces may have also enhanced silica fluxes to Cretaceous seawater (Coltice et al., 2013; Müller et al., 2008; Gaffin, 1987). A silica proxy would better corroborate the hypothesis of whether silica rich Cretaceous seas led to the independent acquisition of a siliceous skeleton in several taxa during this time. No seawater silica proxy currently exists, therefore research was undertaken in this thesis to identify a potential silica proxy. First, correlations between silica and other chemical species in dissolved cation or polyanion form in riverine water and hydrothermal fluids were searched for. Then the robust $^{87}Sr/^{86}Sr$ seawater record was explored as a potential silica proxy.

V. The Search for a Silica Proxy

A. Linear Regressions of Riverine Si vs. Other Ions/Variables

1. Linear Regressions of Global Riverine Data from Gaillardet et al. 1999

Riverine input is a significant source of marine silica today and probably was in the past as well. It is therefore important to explore possible silica proxies using modern riverine data so they may be used to constrain ancient riverine silica fluxes to the ocean. Regression analyses using global riverine data and data on rivers draining smaller monolithological

catchments were used in the search for a riverine silica proxy.

Global riverine data for 60 of the world's largest rivers were compiled by Gaillardet et al. (1999), where 'large' is defined by the dissolved load in 10^6 tons year^{-1}. This dataset includes the concentrations of the major ions Na, K, Ca, Mg, Cl, SO_4, HCO_3, and SiO_2. In addition, the values on river basin area, discharge, runoff, total dissolved solids, and total suspended solids are reported. These data are from the GEMS/WATER Global Register of River Inputs (GEMS/GLORI) compiled by Meybeck & Ragu (1997). This database contains water quality information on approximately 550 rivers with exorheic basins over 10,000 km^2 and discharges exceeding 10 km^3 year^{-1} (Gaillardet et al., 1999). $^{87}Sr/^{86}Sr$ values and Sr concentrations are also reported, though values are present only for roughly half of the rivers. Strontium concentrations and $^{87}Sr/^{86}Sr$ values were compiled from various sources (Gaillardet et al., 1999 and references therein).

Regression analyses of all variables were made against riverine silica concentrations or fluxes to determine if silica is highly correlated with any other major ion or riverine variable on a global scale. The R^2 values, which show how well the data fit to the regression line and therefore how well each variable linearly correlates with others, are presented in Table 5.

Riverine Variable	R^2 values with SiO_2 (μmol L^{-1})
Area (10^6 km^2)	0.0
Discharge (km^3 yr^{-1})	0.0
Runoff (mm yr^{-1})	0.03
TDS (mg L^{-1})	0.05
TSS (mg L^{-1})	0.11
Na (μmol L^{-1})	0.02
K (μmol L^{-1})	0.0
Ca (μmol L^{-1})	0.11
Mg (μmol L^{-1})	0.03
Cl (μmol L^{-1})	0.04
SO_4 (μmol L^{-1})	0.11
HCO_3 (μmol L^{-1})	0.04
Sr (μmol L^{-1})	0.05
$^{87}Sr/^{86}Sr$	0.06

Table 5. R^2 values of riverine Si concentrations versus other reported riverine variables for the largest rivers worldwide. Data used to perform the linear regressions are from Gaillardet et al. 1999.

No riverine variables listed in Table 5 show a high or even moderate linear correlation with riverine silica concentrations. Riverine calcium concentrations have the highest R^2 value, with an insignificant 0.11. The lowest R^2 value with silica is area, showing essentially no correlation. Based on the variables measured in Gaillardet et al. (1999), no proxy for riverine silica concentrations on a global scale was identified.

A linear regression of Na and K concentrations from the global riverine dataset was performed to instill confidence in the results presented in Table 5. Na and K are both alkali elements and because their behavior is similar, a correlation between the two is expected. The R^2 value of Na vs. K was found to be 0.25. This indicates there is little correlation between Na and K concentrations on a global scale. Indeed, no variables appear to correlate for this global riverine dataset.

These results indicate that it is difficult to identify relationships between variables on a global scale. The reason why no variable correlates with riverine silica on a global scale is perhaps due to the great variation in riverine basin lithologies, for the rates of weathering

and dissolved ions released from the weathering of different rock types vastly differs. It is possible that riverine silica concentrations would show better correlations with other dissolved ions from riverine data draining predominantly a single or major lithologic type of fixed or relatively restricted composition. This is because the rate of weathering and the dissolved load would be more uniform. To test this hypothesis, regressions of riverine silica concentrations with other ion concentrations were carried out using the datasets of rivers draining dominantly one lithology. Riverine basins draining predominantly granitoid rocks and basalts were chosen, for an abundant amount of river chemistry data is available in the literature.

2. Linear Regressions of Riverine Water Draining Granitoids

Two datasets were used to carry out regression analyses between silica and other solutes for rivers draining predominantly granitoid rocks. Blum et al. (1998) reported the major ion concentrations of Ca, K, Mg, Si, Sr, and HCO_3^- in rivers of the Himalayan Raikhot watershed, which drains predominantly granites and gneisses. In addition, $^{87}Sr/^{86}Sr$ values were reported, though for only seventeen of the twenty-five samples.

The values reported in Blum et al. (1998) include filtered and unfiltered riverine samples. The filtered samples were poured through an acid-washed 0.45 μm polypropylene filter in the field, whereas the unfiltered samples were filtered in the lab 6 to 12 months after the samples were obtained (Blum et al., 1998). The filtered dataset was used to obtain the best results. The R^2 values for filtered samples between riverine silica and the other riverine variables reported in Blum et al. (1998) is presented in Table 6.

Riverine Variable	R^2 value with SiO_2 (µmol/L)
Ca (µmol/L)	0.45
K (µmol/L)	0.06
Mg (µmol/L)	0.11
Na (µmol/L)	0.79
Sr (nmol/L)	0.11
$^{87}Sr/^{86}Sr$	0.40

Table 6. R^2 values of SiO_2 concentrations versus riverine variables for Raikhot watershed filtered water samples. Data used to perform the linear regressions are from Blum et al. 1998.

Sodium concentrations show a strong linear correlation with riverine silica, having a R^2 value of 0.79. Calcium concentrations and $^{87}Sr/^{86}Sr$ values display moderate correlations, having R^2 values of 0.45 and 0.40, respectively. Potassium, magnesium, and strontium concentrations show very little to no correlation with silica concentrations.

The second dataset used to carry out regression analyses between riverine silica fluxes and other reported variables in rivers draining predominantly granitoids is from White & Blum (1995). Granitoids include plutonic granitic rocks and high-grade metamorphic gneisses (White & Blum, 1995). Data on the riverine fluxes of the ions Na, K, Ca, Mg, Cl, and SO_4 in addition to river area, elevation (min), elevation (max), precipitation, runoff, temperature, and pH were reported from sixty-eight watersheds worldwide. The R^2 values of the regressions from the data of White & Blum (1995) are presented in Table 7.

Riverine Variable	R^2 value with SiO_2 (mol ha^{-1} yr^{-1})
Area (ha)	0.01
Elevation (min)	0.04
Elevation (max)	0.04
Precipitation (mm)	0.37
Runoff (mm)	0.38
Temperature (^oC)	0.32
pH	0.02
Na (mol ha^{-1} yr^{-1})	0.62
K (mol ha^{-1} yr^{-1})	0.45
Ca (mol ha^{-1} yr^{-1})	0.09
Mg (mol ha^{-1} yr^{-1})	0.76 (0.51)*
Cl (mol ha^{-1} yr^{-1})	0.49
SO_4 (mol ha^{-1} yr^{-1})	0.03

Table 7. R^2 values for riverine silica concentrations versus riverine variables from sixty-eight watersheds draining granitoid rocks. Data used to perform the linear regressions are from White & Blum 1995. * R^2 value with one outlier removed

Riverine magnesium fluxes have the highest linear correlation with silica fluxes for rivers draining predominantly granitoid rocks according to the dataset compiled by White & Blum (1995), with an R^2 value of 0.76. Upon closer inspection, a significant amount of weight was placed on one outlier data point, the fluxes of Mg and SiO_2 from the Rio Icacos watershed, Puerto Rico, that have high magnesium fluxes (1538 mol ha^{-1} yr^{-1}) and even higher silica fluxes (8066 mol ha^{-1} yr^{-1}) (Fig 8). When this one data point was removed, a R^2 value of 0.51 (Fig. 8) was obtained and this is the R^2 value accepted here.

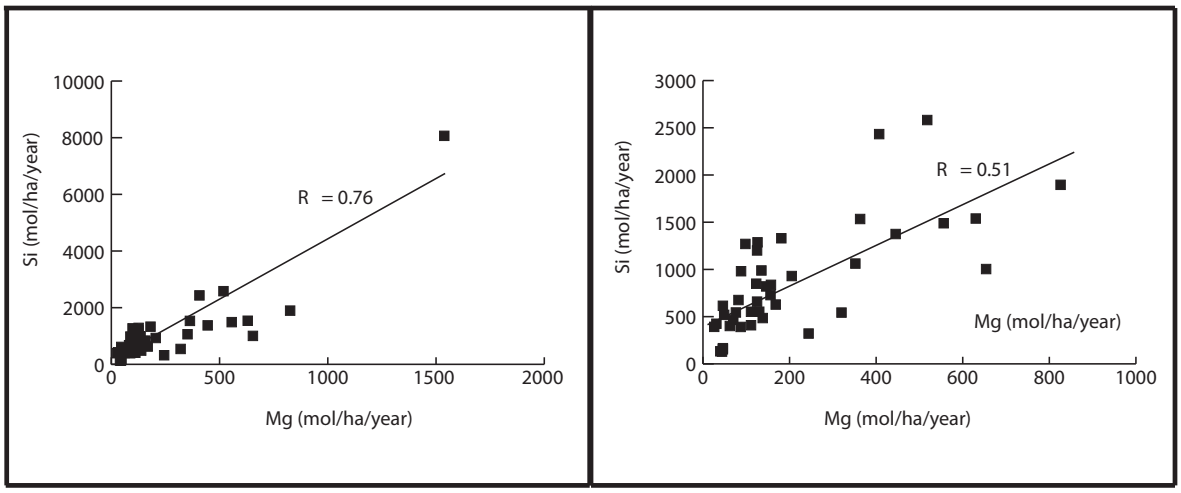

Fig. 8 Linear regression of dissolved magnesium concentrations with dissolved silica concentrations in the Rio Icacos watershed, Puerto Rico. Regression using all available data from White & Blum 1995 (left) and with one outlier removed (right).

Based upon this finding, sodium fluxes once again show the highest degree of correlation with silica fluxes for rivers draining predominantly granitoid rocks, having an R^2 value of 0.62. In addition, chlorine and potassium fluxes show a moderate correlation with silica fluxes, as do runoff, precipitation, and temperature. Area, elevation (minimum and maximum), pH, Ca, and SO_4 show no correlation with silica.

Based on the regression analyses performed on both datasets of rivers draining predominantly granitoid rocks, a strong correlation between silica and sodium was found. The R^2 value of 0.62 for silica and sodium fluxes found using the data of White & Blum (1995) is especially striking considering their dataset includes 68 globally distributed watersheds. The R^2 value of 0.79 for silica and sodium fluxes from the Raikhot watershed further supports this conclusion. There was no correlation found between riverine silica and sodium on a global scale, having an R^2 value of 0.02. This finding supports the hypothesis that relationships between dissolved silica and other dissolved species or variables may exist for monolithological river basins, yet these relationships may be obscured by lithologically varied riverine basins worldwide due to averaging over different kinds of rocks.

3. Linear Regressions of Riverine Water Draining Basalts

Two datasets were used to carry out regression analyses on small catchments draining predominantly basalts. Riverine data of the main streams on Réunion Island draining mafic volcanics (intermediate between tholeiitic and alkaline basalts) were taken from Louvat & Allegre (1997). The concentrations of the ions HCO_3, Cl, SO_4, Na, Ca, Mg, K, Sr, Rb, Ba, B, and Li were reported, in addition to temperature, pH, and $^{87}Sr/^{86}Sr$ values. The R^2 values for the regression analyses from this dataset are presented in Table 8.

Riverine Variable	R^2 values with SiO_2 (µM)
HCO_3 (µM)	0
Cl (µM)	0.06
SO_4 (µM)	0.02
Na (µM)	0.02
Ca (µM)	0.02
Mg (µM)	0
K (µM)	0.28
Sr (nM)	0.03
Rb (nM)	0.44
Ba (nM)	0.01
B (nM)	0.11
Li (nM)	0.02
Temperature (^oC)	0
pH	0
$^{87}Sr/^{86}Sr$	0.07

Table 8. R^2 values of silica concentrations versus other reported variables for rivers draining predominantly basalt on Réunion island. Data used to perform linear regressions was taken from Louvat & Allegre 1997.
Allegre 1997.

No variable in Table 8 shows a strong correlation with silica concentrations. Rubidium shows the highest correlation, with a R^2 value of 0.44, and potassium shows the next highest R^2 value, with a weak 0.28. All of the other variables show no correlation, with several variables having a R^2 value of zero.

Data from rivers draining the predominantly alkali basaltic (White et al., 1979) terrain of the Sao Miguel Island taken from Louvat & Allegre (1998) was the second dataset

used in the regression analysis. The concentrations of several major and trace elements in five rivers were documented; these include HCO_3, Cl, SO_4, F, Br, NO_3, PO_4, Na, K, Mg, Ca, Al, Li, Rb, Sr, and Ba. Riverine temperature and pH values were also reported. Though data for five rivers were available, only data from four of the rivers were used in the regression analyses. Data on the Ribeira Grande River were excluded because many of the values reported for each variable were outliers and skewed the R^2 values for many analyses. This probably suggests that ground water seeps may contribute to the riverine discharge.

Riverine Variable	**R^2 value with SiO_2 (µmol/L)**
T(^{o}C)	0.07
pH	0.86
HCO_3 (µmol/L)	0.96
Cl (µmol/L)	0.98
SO_4 (µmol/L)	0.71
F (µmol/L)	0.03
Br (µmol/L)	0.98
NO_3 (µmol/L)	0.65
PO_4 (µmol/L)	0.69
Na (µmol/L)	0.92
K (µmol/L)	0.31
Mg (µmol/L)	0.93
Ca (µmol/L)	0.89
Al (µmol/L)	0.02
Li (µmol/L)	0.07
Rb (µmol/L)	0.16
Sr (µmol/L)	0.96
Ba (µmol/L)	0.86
Cs (µmol/L)	0
$^{87}Sr/^{86}Sr$	0.19

Table 9. R^2 values of silica concentrations and riverine variables for four rivers draining alkali basalts of Sao Miguel.

Several variables showed a strong correlation with silica. HCO_3, Cl, Br, Na, Mg, and Sr concentrations all have R^2 values exceeding 0.9. Calcium concentrations, barium concentrations, and pH values also show a strong correlation, having R^2 values of 0.89, 0.86, and 0.86, respectively. SO_4, NO_3, and PO_4 correlate quite well with SiO_2 and the

concentrations of Fl, K, Al, Li, Rb, Cs, temperature and $^{87}Sr/^{86}Sr$ values all have little to no correlation with silica concentrations.

While there are many variables that correlate quite strongly for this dataset, the calculated R^2 values may not be as robust as those of Réunion Island because data for only four rivers were available, whereas the Réunion Island dataset contains 53 samples from six rivers. The basaltic composition of Réunion and Sao Miguel islands do not vastly differ and the significant difference in R^2 values between the two datasets is not likely due to lithology.

In summary, sodium has the greatest potential as a proxy for riverine silica input from the weathering of granitoids. High abundances of sodium are present in evaporites, namely halite, which have little to no silica and weather much more rapidly than granite. If halite were present in a watershed this would make sodium a poor proxy for riverine silica to seawater from the weathering of granites. No proxy for silica from rivers draining basalt was found, for the R^2 values from both analyses varied greatly. Linear regression analyses using more datasets may help to identify a silica proxy for rivers draining basaltic terrain. This would be a fruitful area of research because basalt releases a significant quantity of silica at a fast rate compared to other silicate rocks (Jansen et al., 2010).

4. Linear Regressions of Hydrothermal Fluids

Hydrothermal vents are the third greatest source of dissolved silica to seawater after riverine input (dissolved inorganic and biogenic) and seafloor weathering, with an annual flux of 0.6 ± 0.4 Tmol $year^{=1}$, (Treguer & De La Rocha, 2012). The flux of silica from hydrothermal vents has likely varied throughout geologic history.

Linear regression analyses were performed using modern hydrothermal data from three sources in the search for a hydrothermal silica proxy. Three datasets were used to

increase the confidence in the R^2 value obtained. A linear regression analysis was performed between silica and strontium concentrations in vent fluids because strontium concentrations have great potential to act as a hydrothermal silica proxy when coupled with the $^{87}Sr/^{86}Sr$ record. This is because hydrothermal $^{87}Sr/^{86}Sr$ values are very low, thus low $^{87}Sr/^{86}Sr$ values in the geologic past likely indicates that a greater flux of strontium was delivered to seawater from hydrothermal sources than from the weathering of carbonate and silicate rocks. If strontium concentrations and silica concentrations are highly correlated in hydrothermal fluids then this would indicate that a significant amount of silica came from hydrothermal sources.

Silica and strontium concentrations in hydrothermal fluids were first taken from Michard et al. (1984), who report major and trace element concentrations in hydrothermal fluids from the 13^o N East Pacific Rise hydrothermal vent site. Seven samples were obtained from black smoker fluids and two samples were obtained from white smokers. Only the samples from the black smokers were used in the regression analysis due to the sparseness of data for the white smokers. The R^2 value of 0.7 indicates that strontium and silica concentrations have a strong correlation according to this dataset (Fig. 9).

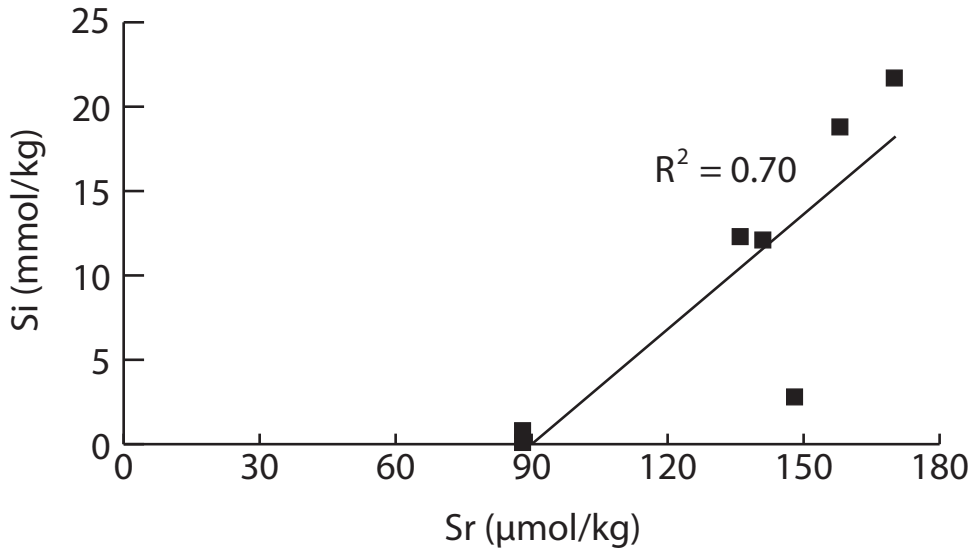

Fig. 9 Linear regression of strontium and silica concentrations in hydrothermal vent fluids from 13° N East Pacific Rise hydrothermal vent site. Michard et al. 1984.

The second source of silica and strontium concentrations in hydrothermal fluids was Schmidt et al. (2007), who reported the concentrations of several major and trace elements in hydrothermal fluids from the ultramafic-hosted Logatchev hydrothermal vent site at 15° N on the Mid Atlantic Ridge. Measured concentrations and endmember concentrations are available for six samples, yet only the measured concentrations were used in the regressions to determine the most accurate R^2 value.

The R^2 value from the dataset of Schmidt et al. (2007) was 0.9 (Fig. 10). These results indicate strontium and silica concentrations in hydrothermal fluids have a strong linear correlation.

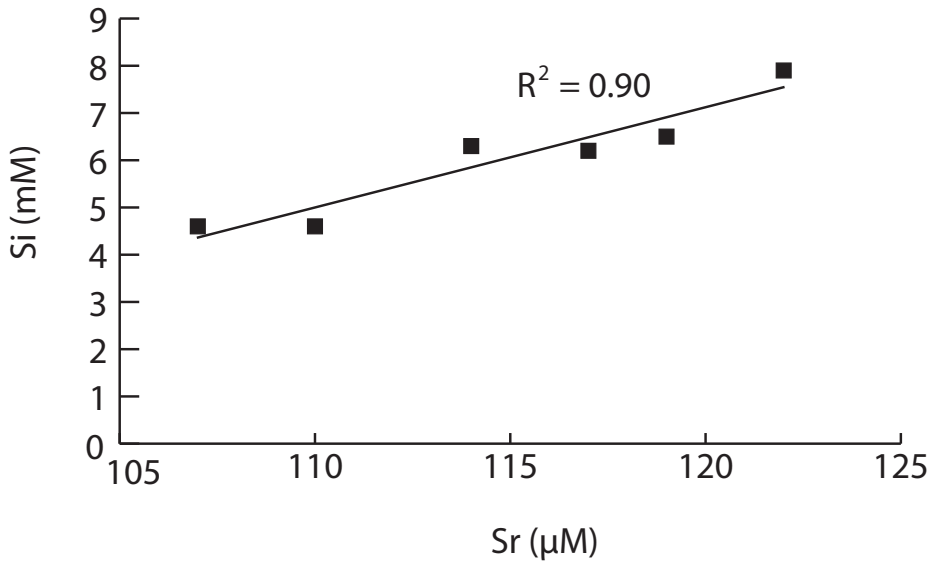

Fig. 10 Linear regression of strontium and silica concentrations in hydrothermal vent fluids from Logatchev hydrothermal vent site 15° N Mid Atlantic Ridge. Schmidt et al. 2007

The last source of silica and strontium concentrations was Von Damm (2000), who reports the concentrations of twelve major and trace element concentrations in hydrothermal fluids from ten vents immediately post-eruptive located from 9°-10° N on the East Pacific Rise. The endmember concentrations for silica and strontium are only available and are therefore used in the linear regression.

The R^2 value calculated from Von Damm (2000) has the lowest value (0.46) of all three datasets used for silica and strontium concentrations. It is unknown why this dataset does not show as strong of a linear relationship at the other two datasets. This may be because the Von Damm dataset consists of endmember data and not measured data, as Michard et al. (1984) and Schmidt et al. (2007) provide.

Silica and strontium concentrations in hydrothermal vents appear to be a good proxy for silica from hydrothermal sources because two datasets show a strong linear correlation between silica and strontium concentrations and the third dataset shows a moderate correlation.

When coupled with the $^{87}Sr/^{86}Sr$ record through time, this finding may be useful for determining whether hydrothermal silica fluxes may have been high for the Cretaceous. Hydrothermal $^{87}Sr/^{86}Sr$ values are very low (~0.7040) and if the $^{87}Sr/^{86}Sr$ seawater curve is controlled by the fluxes of strontium from the continental weathering of silicates, carbonates, and hydrothermal vents, (Brass, 1976) then times when $^{87}Sr/^{86}Sr$ values were low would indicate a greater flux of strontium from hydrothermal sources, and also silica based upon the findings here. Indeed the Cretaceous shows some of the lowest $^{87}Sr/^{86}Sr$ values of the Phanerozoic, reaching as low as 0.70721 at 115 Ma. Yet, the lowest $^{87}Sr/^{86}Sr$ value of the Phanerozoic was during the middle Jurassic, reaching 0.70683 at 168 Ma.

Low $^{87}Sr/^{86}Sr$ values are also characteristic of continental basalts, with the same $^{87}Sr/^{86}Sr$ value of 0.7040 as seafloor volcanics (Brass, 1976). Weathering of a vast amount of continental basalts may also cause $^{87}Sr/^{86}Sr$ values to decrease by releasing large quantities of non-radiogenic strontium to seawater. No continental flood basalts were emplaced during the Cretaceous except for the Deccan Traps at the Cretaceous – Paleogene boundary (Fig. 5) and the continental flood basalts that were emplaced closest to the beginning of the Cretaceous were the Karoo-Ferrar (185 – 175 Ma; Bryan & Ernst, 2008) and the Central Atlantic Magmatic Province (205 – 191 Ma; Bryan & Ernst, 2008). Based upon these findings and the evidence from the seawater $\delta^{34}S$ record indicating hydrothermal activity was heightened during the Cretaceous (Paytan et al., 2004), the low $^{87}Sr/^{86}Sr$ during this time was likely due to increased seafloor spreading activity. The emplacement of the voluminous ocean basin flood basalt provinces and the increased seafloor production during the Cretaceous are temporally aligned with the low $^{87}Sr/^{86}Sr$ values.

Based upon the above findings, the $^{87}Sr/^{86}Sr$ record along with the linear correlation

between strontium and silica concentrations in hydrothermal fluids appears to be a good candidate for a seawater silica proxy. This premise is contingent upon an accurate model that explains the variables responsible for changes in the $^{87}Sr/^{86}Sr$ record. Two models are the next topic of discussion. First, a simple, older model is presented and then, a more complex model that explains the $^{87}Sr/^{86}Sr$ curve is presented.

B. $^{87}Sr/^{86}Sr$ as a silica proxy

There is currently no proxy for tracking silica fluxes to the ocean for the geologic past. The $^{87}Sr/^{86}Sr$ curve is a well-known seawater record with robust data available for the past two hundred million years. Because of this, it was explored as a possible seawater silica proxy. In order to determine if ancient $^{87}Sr/^{86}Sr$ values can be used as a silica proxy and answer if silica inputs to Cretaceous oceans were heightened, it is necessary to first understand the variables controlling changes in the $^{87}Sr/^{86}Sr$ curve. The $^{87}Sr/^{86}Sr$ value on short time scales (thousands of years) is homogenous throughout the ocean, yet on longer geologic time scales (the order of millions of years) the $^{87}Sr/^{86}Sr$ record has varied greatly (Fig. 6a). The change in the $^{87}Sr/^{86}Sr$ record over millions of years is due to changes in the fluxes of strontium from its major sources (Brass, 1976). Two models that attempt to explain the $^{87}Sr/^{86}Sr$ are presented. First, an older, simple model from 1965 (Faure et al., 1965) is presented and then a more recent and complex model from 1976 (Brass, 1976) is covered. A variable present in each model is solved for and the results are then compared to independently derived data to test the robustness of each model.

1. Faure et al. 1965 $^{87}Sr/^{86}Sr$ Model

Faure and others in their 1965 paper created a simple mixing model to explain the modern seawater $^{87}Sr/^{86}Sr$ value of 0.70918. They recognized three different sources of

strontium to seawater, each with a distinct $^{87}Sr/^{86}Sr$ ratio. Seafloor volcanics, which includes mid-ocean ridge basalts, ocean island basalts, ocean basin flood basalt provinces, and island arc volcanics, are a major source of seawater strontium, with a low $^{87}Sr/^{86}Sr$ value of 0.7040. Continental silicate rocks are another major source of strontium, with a high $^{87}Sr/^{86}Sr$ value of 0.7200. This is because sialic rocks are enriched in ^{87}Rb, which decays to ^{87}Sr. The dissolution of marine carbonates also contributes a significant amount of strontium to seawater, having an intermediate $^{87}Sr/^{86}Sr$ value of 0.7080. The $^{87}Sr/^{87}Sr$ values through time can therefore be explained according to this model based upon variations in the fraction of strontium delivered to seawater from each source.

The model assumes that the fraction of strontium from marine carbonates (m_o) has been constant throughout the Phanerozoic, delivering between 60% - 80% of strontium to the oceans. With the strontium from marine carbonates set as a constant, the variations seen in $^{87}Sr/^{86}Sr$ throughout time are, in this model, due to changes in the fraction of strontium delivered from volcanic sources (v) and the fraction of strontium from the weathering of sialic continental rocks (s). When $^{87}Sr/^{86}Sr$ values are high, it is expected that the fraction of strontium from volcanic sources is low and those from sialic sources high. Likewise, when $^{87}Sr/^{86}Sr$ values were low, it is expected that the fraction of strontium from volcanics was high and that from sialic continental sources low.

To determine if the $^{87}Sr/^{86}Sr$ curve can be interpreted as changes in the fraction of strontium delivered from volcanic and sialic sources, the fraction of strontium delivered to seawater from volcanic sources (v) was calculated for the past 200 million years (Fig. 11).

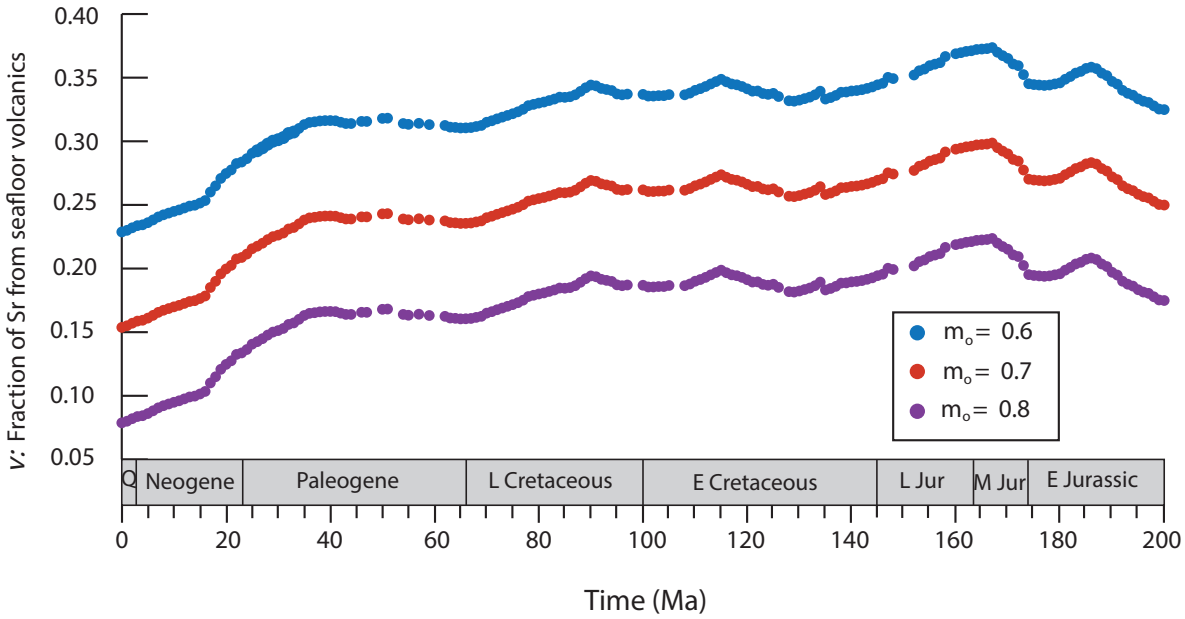

Fig. 11 Calculated v (the fraction of strontium from seafloor volcanics) when m_o (the fraction of strontium from the weathering of marine carbonates) is 0.6, 0.7, and 0.8 for the past 200 Ma using the model of Faure et al. 1965.

Three curves were generated, each calculated with marine carbonates delivering 60%, 70%, or 80% of strontium to seawater. The fraction of strontium delivered from seafloor volcanics when m_o = 0.7 was then graphed alongside the $^{87}Sr/^{86}Sr$ curve and the average seafloor production rate curve from Fig. 5. The m_o = 0.7 curve was chosen because it is the intermediate curve and would produce the best results.

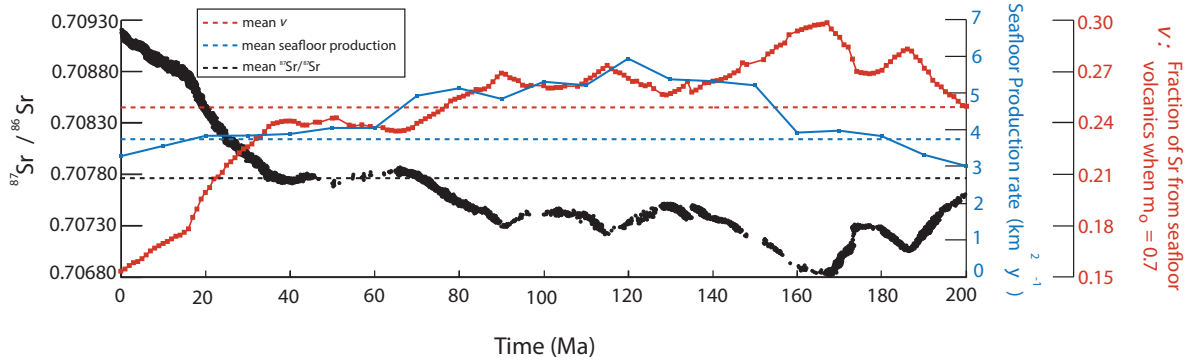

Fig. 12 The $^{87}Sr/^{86}Sr$ seawater curve (black), calculated v curve (red), and the mean seafloor production rate curve (blue) for the past 200 Ma. The mean for each of these curves are shown with a dotted line for the past 200 Ma.

The fraction of strontium delivered to seawater from seafloor volcanics increases when the generation of oceanic crust is high and this fraction decreases when seafloor crustal production is low. The seafloor crust production rate should thus correlate well with the calculated *v* term. Likewise, $^{87}Sr/^{86}Sr$ values should show a predictive trend with seafloor crust production rates if the Faure et al. model's assumptions are correct. $^{87}Sr/^{86}Sr$ values should be low when seafloor crust production rates are high because oceanic crust has a low $^{87}Sr/^{86}Sr$ value of 0.7040 and $^{87}Sr/^{86}Sr$ values should be high when the seafloor crust production is low and a greater fraction of strontium is coming from continental sialic sources because their $^{87}Sr/^{86}Sr$ values are higher.

To determine the robustness of Faure et al.'s model, the calculated *v* was compared to other independently derived measures of seafloor production rates (Fig. 12). Calculated *v* was compared to the mean seafloor production rate curve (Fig. 5) calculated from the seafloor production rate curves of Coltice et al. (2013), Müller et al. (2008), and Gaffin (1987).

The mean fraction of strontium delivered to the oceans from the weathering of volcanic rocks (*v*) when the fraction of marine carbonates is kept at the constant 0.7 for the past 200 million years is 0.25. The fraction of strontium delivered to the oceans from volcanic sources was below 0.25 from 0 – 77 Ma and is above the mean from 78 – 200 Ma.

The mean seafloor production rate for the past 200 million years, calculated from the mean seafloor production rate from Fig. 5 is 3.77 $km^2\ Myr^{-1}$. The rate of seafloor production is below the mean from 0 – 63 Ma and 157 – 200 Ma. The rate of seafloor production is above its mean from 63 – 157 Ma (Fig. 12).

Calculated *v* and the mean seafloor production rate curve show the same trend from

0 – 63 Ma, with each below their means, and they also agree from 78 – 157 Ma when each curve is above their respective mean. These two curves show the same trend for 142 million years out of the past 200 million years. Times when seafloor production rate and *v* do not show similar trends about the mean are from 63 – 77 Ma, when the mean seafloor production rate curve was above its mean and calculated *v* was below its mean. From 157 – 200 Ma they also differ: seafloor production was below its mean and v was above its mean. Each curve displays the opposite trend about the mean for a total of 58 million years from the past 200 million years.

Because *v* was calculated from the $^{87}Sr/^{86}Sr$ curve, the $^{87}Sr/^{86}Sr$ curve will agree and disagree with the seafloor production rate curves during the same time intervals as the calculated *v* curve did. Because of this, it is not necessary to compare the $^{87}Sr/^{86}Sr$ curve with the seafloor production rate curves.

Calculated *v* when $m_o = 0.7$ for the past 200 Ma does not agree with the mean seafloor production rate curve 30% of this time. This indicates that the Faure et al. model may not be a robust model for explaining changes in the $^{87}Sr/^{86}Sr$ seawater curve. Indeed, a major flaw of this model is that the rate of change is not incorporated. Therefore, the Faure et al. model is not an accurate $^{87}Sr/^{86}Sr$ model and it cannot be used as a step to determine if the $^{87}Sr/^{86}Sr$ curve is a good proxy for silica fluxes to seawater through time. The model of Brass (1976) is next explored as an accurate $^{87}Sr/^{86}Sr$ model which takes into account the rate of change of $^{87}Sr/^{86}Sr$ values for the Phanerozoic.

2. Brass 1976 $^{87}Sr/^{86}Sr$ Model

Brass created a two component model that explains the rate of change in the $^{87}Sr/^{86}Sr$ curve for the past four hundred million years. Like Faure et al. (1965), Brass recognized that

older continental silicate rocks, marine carbonates, and young basic rocks such as basalts each have distinct $^{87}Sr/^{86}Sr$ values. These values are 0.7200, 0.7080, and 0.7040, respectively, and are nearly the same as those reported in Faure et al. (1965). Brass claims that the changes in $^{87}Sr/^{86}Sr$ seawater values through time are caused by changes in the proportion of different lithologies that are weathered. Like Faure et al. (1965), Brass (1976) assumes the weathering of carbonates has been relatively constant and therefore fluctuations in $^{87}Sr/^{86}Sr$ values are ultimately from changes in the proportion of strontium from old silicate rocks and younger basic rocks. The model of Brass does not incorporate strontium from oceanic volcanics as Faure et al. did, claiming that seafloor basalts are a sink and not a source of seawater strontium based upon the limited data from Hart (1969) and Hart & Nalwalk (1970).

The model explains the rate of change in the $^{87}Sr/^{86}Sr$ curve $\left(\frac{dR_{SW}}{dt}\right)$ by taking into account the $^{87}Sr/^{86}Sr$ value of rivers draining predominantly carbonates (R_{ls}) and older sialic rocks + continental basalts (R_{cc}), the concentration of strontium in each of these waters ($\{Sr_{ls}\}$, $\{Sr_{cc}\}$), and the riverine flux of each to seawater (F_{ls}, F_{cc}). The $^{87}Sr/^{86}Sr$ value of modern seawater (R_{SW}), the concentration of strontium in seawater today ($\{Sr_{SW}\}$), and the volume of the ocean (V) were also incorporated into the model.

Changes to the Brass model were made in order to create a model that explains the rate of change in $^{87}Sr/^{86}Sr$ values through time. Older silicate rocks, younger continental basalts, and other non-carbonate rocks were grouped into one component. The $^{87}Sr/^{86}Sr$ value of this component was estimated to be 0.7190 because the $^{87}Sr/^{86}Sr$ of older silicate rocks is 0.7200 and the $^{87}Sr/^{86}Sr$ of young basalts is 0.7040, yet today basic continental volcanics represent ~6% of Earth's exposed continents (Dürr et al., 2005). The concentration of strontium in riverine water draining silicate rocks and basalts was adjusted to 0.06 μM

based upon the small exposure of basalts on Earth's continents. A hydrothermal component was added because contrary to what Brass claims, several studies have since confirmed that hydrothermal vents along mid-ocean ridges are indeed a source of seawater strontium (e.g. Schmidt et al., 2007; Von Damm, 2000; Michard et al., 1984; Edmond et al., 1982). The $^{87}Sr/^{86}Sr$ value of hydrothermal fluids (R_{MORB}), the concentration of strontium in these fluids ($\{Sr_{MORB}\}$), and the flux of water that circulates through the ocean floor along mid-ocean ridges (G) were incorporated. In addition, variables representing the flux of riverine water draining carbonates (F_{ls}) and the flux of riverine water draining non-carbonates(F_{cc}) were included in the model. Further detail concerning the Brass model is shown in the Appendix.

To determine the robustness of the Brass model's ability to explain the rate of change in the $^{87}Sr/^{86}Sr$ curve for the past 200 Ma, an unknown variable X was solved for and the result was then used to solve for the flux of water circulating through oceanic crust at mid-ocean ridges (G). It is assumed that the ratio of G to the rate of seafloor production through time is constant and by comparing the calculated G to the independently derived seafloor production curves from Coltice et al. (2013), Müller et al. (2008), and Gaffin (1987), the robustness of the Brass model may be tested.

The variable X is the fraction of the global riverine flux draining non-carbonates. This variable is incorporated into the variable F_{cc}, which has been previously introduced. Because the global riverine flux is broken into two components, the flux from rivers draining carbonates (F_{ls}) and the flux from rivers draining non-carbonates (F_{cc}), the variable F_{cc} can be set to equal X multiplied by F and F_{ls} can be set to equal (1 – X)F. F is the global riverine flux (x 10^6 km^3 My^{-1}) and these values for throughout the Phanerozoic are from Tardy et al. (1989) (Table 10).

To calculate X, the flux of water circulating through oceanic crust at mid-ocean ridges (G) must first be known. G was calculated by assuming the ratio of the global hydrothermal flux to the rate of seafloor production has been constant throughout geologic history. The global hydrothermal flux of today was taken to be 2 x 10^{13} kg/yr, which is on the lower end of the range of 2 – 6 x 10^{13} kg/yr provided by (Bach et al., 2013) and the volume of oceanic crust being produced today is 20 km^3/yr based upon Fig. 6. Using these values, it was calculated that for every one kilogram of water from hydrothermal sources going into the ocean each year, three kilograms of oceanic crust is produced. Yet, oceanic crust is approximately three times as dense as the water emanating from hydrothermal vents and therefore, the emplacement rate of mid-ocean ridge basalt in 10^6 km^3 Myr^{-1} have the same values as the global hydrothermal flux in 10^6 km^3 Myr^{-1} (Fig. 6).

The rate of change in the $^{87}Sr/^{86}Sr$ curve $\left(\frac{dR_{SW}}{dt}\right)$ for the past 200 Ma was also required to calculate the variable X. The rate of change was calculated in ten million year intervals because the global hydrothermal flux values were known every ten million years for the past 200 Ma. The rate of change values are presented in Table 10. All of the other values to calculate X were taken from the literature and are present in Table 10.

Time (Ma)	dR_{SW}/dt	R_{Is}	R_{SW}	$\{Sr\}_{Is}$ (μM)	$\{Sr\}_{SW}$ (μM)	F (10^6 km^3 My^{-1})	V (10^9 km^3)	R_{CC}	$\{Sr_{CC}\}$	R_{MORB}	$\{Sr\}_{MORB}$ (μM)	G (10^6 km^3 My^{-1})
0	———	0.7080	0.70918	4	87		1.335	0.7190	0.06	0.7040	119	2.83
10	-2.46E-05	0.7080	0.70918	4	87	41.45	1.335	0.7190	0.06	0.7040	119	3.07
20	-6.26E-05	0.7080	0.70918	4	87	41.45	1.335	0.7190	0.06	0.7040	119	3.30
30	-3.61E-05	0.7080	0.70918	4	87	45.27	1.335	0.7190	0.06	0.7040	119	3.31
40	-3.64E-06	0.7080	0.70918	4	87	49.44	1.335	0.7190	0.06	0.7040	119	3.35
50	4.12E-06	0.7080	0.70918	4	87	49.44	1.335	0.7190	0.06	0.7040	119	3.49
60	4.58E-06	0.7080	0.70918	4	87	51.88	1.335	0.7190	0.06	0.7040	119	3.49
70	-1.79E-05	0.7080	0.70918	4	87	51.96	1.335	0.7190	0.06	0.7040	119	4.24
80	-2.06E-05	0.7080	0.70918	4	87	51.96	1.335	0.7190	0.06	0.7040	119	4.42
90	-4.28E-06	0.7080	0.70918	4	87	51.96	1.335	0.7190	0.06	0.7040	119	4.17
100	8.02E-07	0.7080	0.70918	4	87	47.46	1.335	0.7190	0.06	0.7040	119	4.56
110	-1.92E-05	0.7080	0.70918	4	87	47.46	1.335	0.7190	0.06	0.7040	119	4.49
120	1.77E-05	0.7080	0.70918	4	87	47.46	1.335	0.7190	0.06	0.7040	119	5.11
130	7.16E-06	0.7080	0.70918	4	87	47.46	1.335	0.7190	0.06	0.7040	119	4.62
140	-1.79E-05	0.7080	0.70918	4	87	42.53	1.335	0.7190	0.06	0.7040	119	4.58
150	-2.41E-05	0.7080	0.70918	4	87	40.48	1.335	0.7190	0.06	0.7040	119	4.49
160	-2.08E-05	0.7080	0.70918	4	87	40.48	1.335	0.7190	0.06	0.7040	119	3.38
170	4.47E-05	0.7080	0.70918	4	87	38.51	1.335	0.7190	0.06	0.7040	119	3.43
180	-2.03E-05	0.7080	0.70918	4	87	38.51	1.335	0.7190	0.06	0.7040	119	3.30
190	3.82E-05	0.7080	0.70918	4	87	40.9	1.335	0.7190	0.06	0.7040	119	2.86
200	———	0.7080	0.70918	4	87	40.9	1.335	0.7190	0.06	0.7040	119	2.60

Table 10. The values used to calculate X in the Brass 1976 model. R_{Is}, R_{SW}, and R_{MORB} are from Brass et al. 1976. Refer to the text for the values of R_{CC} and $\{Sr\}_{CC}$. $\{Sr\}_{Is}$ is from Krabbenhöft et al. 2010, $\{Sr\}_{SW}$ is from Von Damm 1990, F values are from Tardy et al. 1987, V is from www.ngdc.noaa.gov, $\{Sr\}_{MORB}$ is from an average of the values in Michard et al. 1984 and Douville et al. 2002. All other values were calculated in this study.

The variable X at 10 Ma yielded a value of 46.1, which is incorrect considering X should be a fraction. The erroneous X value can be explained by a false assumption the Brass model makes. The greatest source of non-radiogenic strontium to seawater was assumed to come from hydrothermal vents along mid-ocean ridges, yet evidence shows this to be incorrect, with the majority of non-radiogenic strontium to seawater coming from non-axial sources on the seafloor (Galy et al., 1999).

Futhermore, there is evidence that indicates the source of radiogenic strontium is not limited to older continental silicate rocks, as the models of both Faure et al. and Brass claim. Blum et al. (1998) found that the majority of radiogenic strontium in the predominantly silicate Raikhot watershed within the High Himalayan Crystalline Series was in fact derived from trace amounts of carbonate in the bedrock. The radiogenic strontium in these carbonates is thought to come from reequilibrating with silicates having high $^{87}Sr/^{86}Sr$ values during metamorphism (Palmer & Edmond, 1992). Oliver et al. (2003) support the findings of Blum et al. (1998), showing that carbonate weathering is responsible for the supply of highly radiogenic strontium in the Bhote Kosi-Sun Kosi watershed, a major Hiamalayan tributary to the Ganges. Based upon these findings, the $^{87}Sr/^{86}Sr$ is not a good potential proxy for seawater silica because the weathering of carbonates and the weathering of old silicate rocks may both be a source of highly radiogenic strontium to seawater. Therefore, continental weathering of older silicate rocks and their fluxes of dissolved species, including silica, cannot be traced from the $^{87}Sr/^{86}Sr$ record because some carbonates have been found to also have high $^{87}Sr/^{86}Sr$ values.

VI. Conclusions

The Cretaceous was a unique period in the history of siliceous taxa and ocean basin magmatic processes. Evidence presented in this thesis suggests the two phenomena may be linked, with seafloor sources delivering greater quantities of silica to Cretaceous seas than those of the Jurassic or post Cretaceous. This may have made silica a favorable material for skeletal construction during this time.

Oceanic crust production was higher during the Cretaceous than during the Jurassic or post-Cretaceous based on the two-hundred-million year seafloor record. Three independently derived oceanic crust production rate curves each show the highest rates occurred during the Cretaceous (Fig. 5) and an average of these curves indicates the Cretaceous had approximately 35% percent higher oceanic crust production rates than the Jurassic and approximately 38% percent higher rates than after the Cretaceous. Because greater hydrothermal activity results from faster spreading ridges (Devey et al., 2010; Lupton, 1998; Rüth et al., 2000; Lupton et al., 2004) this would have resulted in greater hydrothermal silica fluxes to seawater.

The oceanic crust production rate curves (Fig. 5 & 6) include the emplacement of ocean basin flood basalt provinces, which were more voluminous during the Cretaceous than any other time in the past 200 Ma. From 88 – 90 Ma and 121 – 124 Ma the rates were exceptionally high, reaching at least 25% and 18% of background mid-ocean ridge basalt production rates. The mechanism for silica delivery from these large igneous provinces, whether via weathering or hydrothermal input remains unknown. It is striking that previous research (Ritterbush et al., 2015) suggests the weathering of a terrestrial large igneous province, the Central Atlantic Magmatic Province, delivered a sufficient quantity of silica to

affect siliceous sponges on a global level during the Jurassic. This event leads one to question: did a similar phenomenon occur during the Cretaceous, with large igneous provinces emplaced on the seafloor rather than underneath the continents? It is also noteworthy to recognize that diatom diversity at the genus level increased at approximately the same times that ocean basin flood basalt province production rates were greatest (Fig. 7). In addition, diatoms, silicoflagellates, and chrysophytes first appear in the fossil record when ocean basin flood basalt province production rates were the highest (Fig. 7). The temporal alignment between siliceous taxa and high oceanic crust production rates may have been due to an increased flux of the nutrient silica to seawater, causing a biotic response.

Continental weathering may have also enhanced silica delivery to seawater during the Cretaceous. The warm weather of the early – mid Cretaceous may have increased riverine fluxes of silica to seawater because warmer temperatures enhance continental weathering (Brady & Carroll, 1994; White & Blum, 1995; White et al., 1999; Brady et al., 1999; Dessert et al., 2003; Oliva et al., 2003). Global runoff was also high during the Cretaceous, yet the highest values were not seen until the late Cretaceous.

No viable silica proxy was found in this study. A linear correlation was found between silica and sodium concentrations in rivers draining predominantly granitoids, yet the presence of high amounts of sodium in evaporites such as halite, which weather more rapidly than granite make this a poor candidate for a silica proxy.

The strong linear correlations found between the concentration of silica and strontium in hydrothermal fluids made strontium, when coupled with the $^{87}Sr/^{86}Sr$ a promising seawater silica proxy. Yet, there is currently no model that is able to accurately explain the changes in $^{87}Sr/^{86}Sr$ values through time based upon variations in the fluxes of

strontium from its sources. The findings of Blum et al. (1998) and Oliver et al. (2003), which showed highly radiogenic strontium can come from older silicate rocks or metamorphosed carbonates may make finding a model than explains the $^{87}Sr/^{86}Sr$ seawater curve from changes in the fluxes of strontium from sources with distinct $^{87}Sr/^{86}Sr$ values exceptionally difficult or impossible. Therefore, without a viable model to explain the $^{87}Sr/^{86}Sr$ record, this robust seawater record cannot be used as a seawater silica proxy.

Finally, an indication of the sensitivity skeletonized taxa have to changes in contemporaneous seawater chemistry is required to determine if enhanced silica fluxes to seawater caused the independent acquisition of a siliceous skeleton in several groups during the Cretaceous. This study has amassed evidence that silica fluxes were likely greater during the Cretaceous than the period before and the time after, yet whether this amount was enough to influence the skeletal mineralogy of organisms is still unknown.

VII. Future Directions

Future research should aim to find a reliable silica proxy that can be used to track ancient seawater silica fluxes. Seawater δ^7Li values may prove to be a good proxy that tracks silica fluxes from continental weathering sources because δ^7Li values indicate the weathering style minerals undergo (congruent versus incongruent) and therefore provides a measure of the intensity of continental weathering during a period in time. Research has shown the rise of diatoms during the Cenozoic was due to an increase in continental weathering recorded by the δ^7Li record (Cermeño et al., 2015). δ^7Li data exists for the entire Cenozoic, yet only a few δ^7Li values are known for the Cretaceous (von Strandmann et al., 2013). Future research should aim to determine δ^7Li values for the Mesozoic.

Future studies should also aim to identify the relationship between silica fluxes from

fast versus slow spreading mid-ocean ridges. The silica fluxes are likely greater from faster spreading ridges than slower spreading ridges because larger ^{3}He plumes emanate from faster ridges, (Devey et al., 2010; Lupton, 1998; Rüth et al., 2000; Lupton et al., 2004) but it is not clear what the magnitude of the silica fluxes are. A compilation of silica fluxes from hydrothermal vent sites worldwide that are along mid-ocean ridges with varying spreading rates may show a pattern concerning silica fluxes and seafloor spreading rates.

References

Alexandre, A., Meunier, J-D, Colin, F., Koud, J-M.1997. Plant impact on the biogeochemical cycle of silicon and related weathering processes. *Geochimica et Cosmochimica Acta* 61, 677-682.

Alves, G. M., Velho, L. F., Simões, N. R., Lansac–Tôha, F. A. 2010. Biodiversity of testate amoebae (Arcellinida and Euglyphida) in diferente habitats of a lake in the upper Paraná river floodplain. *European Journal of Protistology* 46, 310-318.

Bach, W., Jöns, N., Klein, F. 2013. Metasomatism within the ocean crust. In: Harlov, D.E., Austrheim, H. (Eds.) *Metasomatism and the Chemical Transformation of Rock*: *The Role of Fluids in Terrestrial and Extraterrestrial Processes.* Springer, Berlin Heidelberg, 253-288.

Bayer, F.M. 1956. Descriptions and redescriptions of the Hawaiian octocorals collected by the US Fish Commission steamer "Albatross"(2. Gorgonacea: Scleraxonia). *Pacific Science* 10, 67-95.

Ben-Avraham, Z., Hartnady, C. J. H., Le Roex, A.P. 1995. Neotectonic activity on continental fragments in the southwest Indian Ocean: Agulhas Plateau and Mozambique Ridge. *Journal of Geophysical Research: Solid Earth (1978–2012)* 100, 6199-6211.

Bengtson, S.S., Conway Morris, S., Cooper, B.J., Jell, P.A., Runnegar, B.N. 1990. Early Cambrian fossils from South Australia. *Memoir of the Association of Australasian Paleontologists* 9, 1-364.

Berger, W., Winterer, E.L. 1974. Plate stratigraphy and the fluctuating carbonate line. In: Hsü, K.J., Jenkyns, H.C., Halam, A. (Eds.) *Pelagic sediments: on land and under the sea*. *Special Publication of the International Association of Sedimentology* 1, 11-48.

Berner, E.K., Berner, R.A. 2004. Plants and Mineral Weathering: Present and Past. In: Drever, J.I. (Ed.) *Treatise on Geochemistry Vol. 5 Surface and Ground Water, Weathering, and Soils*, Elsevier, Spain, 169-188.

Berner, E. K., Berner, R.A. 2012. *Global environment: water, air, and geochemical cycles*. Princeton University Press, Princeton, New Jersey.

Blum, J.D., Gazis, C.A., Jacobson, A.D., Chamberlain, C.P. 1998. Carbonate versus silicate weathering in the Raikhot watershed within the High Himalayan Crystalline Series. *Geology* 26, 411-414.

Bluth, G.J.S., Kump, L.R. 1994. Lithologic and climatologic controls of river chemistry. *Geochimica et Cosmochimica Acta* 58, 2341-2359.

Bohaty, S.M., Harwood, D.M. 2000. Ebridian and silicoflagellate biostratigraphy from Eocene McMurdo erratics and the Southern Ocean. In: Stillwell, J.D., Feldmann, R.M. (Eds.) *Paleobiology and Paleoenvironments of Eocene Rocks: McMurdo Sound, East Antarctica* 76, American Geophysical Union, Washington, 99-159.

Brady, P.V., Carroll, S.A. 1994. Direct effects of CO_2 and temperature on silicate weathering: possible implications for climate control. *Geochimica et Cosmochimica Acta* 58, 1853-1856.

Brady, P.V., Dorn, R.I., Brazel, A.J., Clark, J., Moore, R.B., Glidewell, T. 1999. Direct measurement of the combined effects of lichen, rainfall, and temperature on silicate weathering. *Geochimica et Cosmochimica Acta* 63, 3293-3300.

Brain, C.K., Prave, A.R., Hoffmann, K., Fallick, A.E., Botha, A., Herd, D.A., Sturrock, C., Young, I., Condon, D.J., Allison, S.G. 2012. The first animals: ca. 760-million-year-old sponge-like fossils from Namibia. *S. Afr. J. Sci.* 108, 1-8.

Brasier, M., Green, O., Shields, G. 1997. Ediacarian sponge spicule clusters from southwestern Mongolia and the origins of the Cambrian fauna. *Geology* 25, 303-306.

Brass, G. W. 1976. The variation of the marine $^{87}Sr/^{86}Sr$ ratio during Phanerozonic time: interpretation using a flux model. *Geochimica et Cosmochimica Acta* 40, 721-730.

Braun, A., Chen, J., Waloszek, D., and Maas, A. 2007. First Early Cambrian Radiolaria, In: Vickers-Rich, P., and Komarower, P. (Eds.) *The Rise and Fall of the Ediacaran Biota: Geological Society of London Special Publication* 286, 143-149.

Bryan, S.E., 2005. The Early Cretaceous Whitsunday Silicic Large Igneous Province of eastern Australia. www.largeigneousprovinces.org

Bryan, S. E., Ernst, R.E. 2008. Revised definition of large igneous provinces (LIPs). *Earth-Science Reviews* 86, 175-202.

Bryan, S.E., Cook, A.G., Allen, C.M., Siegel, C., Purdy, D.J., Greentree, J.S., Uysal, I.T. 2012. Early-mid Cretaceous tectonic evolution of eastern Gondwana: From silicic LIP magmatism to continental rupture. *Episodes* 35, 142-152.

Bryan, S.E., Ferrari, L. 2013. Large igneous provinces and silicic large igneous provinces: Progress in our understanding over the last 25 years. *Geological Society of America Bulletin* 125, 1053-1078.

Brzezinski, M. A., Olson, R.J., Chisholm, S.W. 1990. Silicon availability and cell-cycle progression in marine diatoms. *Marine ecology progress series. Oldendorf* 67, 83-96.

Buge, E., Monniot, F. 1972. Nouveaux Spicules D'Ascidiesde L'Ypresien du Bassin de Paris et du Toarcien des Deux-Sevres. *Geobios* 5, 83-90.

Cairns, S.D. 1984. A Generic Revision of the Stylasteridae (Coelenterata: Hydrozoa) Part 2: Phylogenetic Analysis. *Bulletin of Marine Science* 35, 38-53.

Cárdenas, A.L., Harries, P.J. 2010. Effect of nutrient availability on marine origination rates throughout the Phanerozoic eon. *Nature Geoscience* 3, 430-434.

Cao, W., Feng, Q., Feng, F., Ling, W. 2014. Radiolarian *Kalimnasphaera* from the Cambrian Shuijingtuo Formation in South China. *Marine Micropaleontology* 110, 3-7.

Casey, R. E., Cynthia R. W., Perez-Guzman, A. M. 1983. Biogeographic and ecologic perspective on polycystine radiolarian evolution. *Paleobiology* 9*,* 363-376.

Cermeño, P., Falkowski, P.G., Romero, O.E., Schaller, M.F., Vallina, S.M. 2015. Continental erosion and the Cenozoic rise of marine diatoms. *Proceedings of the National Academy of Sciences* 112, 4239-4244.

Coffin, M.F., Pringle, M.S., Duncan, R.A., Gladczenko, T.P., Storey, M., Müller, R.D., Gahagan, L.A. 2002. Kerguelen hotspot magma output since 130 Ma. *Journal of Petrology* 43, 1121-1137.

Coltice, N., Seton, M., Rolf, T., Müller, R.D., Tackley, P.J. 2013. Convergence of tectonic reconstructions and mantle convection models for significant fluctuations in seafloor spreading. *Earth and Planetary Science Letters* 383, 92-100.

Conley, D. J. 2002. Terrestrial ecosystems and the global biogeochemical silica cycle. *Global Biogeochemical Cycles* 16, 68-1-68-8.

Conley, D. J., Carey, J.C. 2015. Biogeochemistry: Silica cycling over geologic time. *Nature Geoscience* 8, 431-432.

Courtillot, V.E., Renne, P.R. 2003. On the ages of flood basalt events. *Comptes Rendus Geoscience* 335, 113-140.

Darley, W. M., Volcani, B.E. 1969. Role of silicon in diatom metabolism: a silicon requirement for deoxyribonucleic acid synthesis in the diatom Cylindrotheca fusiformis Reimann and Lewin. *Experimental Cell Research* 58, 334-342.

Dessert, C., Dupré, B., Gaillardet, J., François, L.M., Allègre, C.J. 2003. Basalt weathering laws and the impact of basalt weathering on the global carbon cycle. *Chemical Geology* 202, 257-273.

Devey, C.W., German, C.R., Hasse, K.M., Lackschewitz, K.S., Melchert, B., Connelly, D.P. 2010. The Relationships Between Volcanism, Tectonism, and Hydrothermal Activity on the Southern Equatorial Mid-Atlantic Ridge. In: Rona, P.A., Devey, C.W., Dyment, J., Murton, B.J. (Eds.) *Diversity of Hydrothermal Systems on Slow Spreading Ocean Ridges,* American Geophysical Union, Washington D.C., 188, 133-152.

Douville, E., Charlou, J.L., Oelkers, E.H., Bienvenu, P., Jove Colon, C.F., Donval, J.P., Fouque, Y., Prieur, D., Appriou, P. 2002. The rainbow vent fluids (36 14′ N, MAR): the influence of ultramafic rocks and phase separation on trace metal content in Mid-Atlantic Ridge hydrothermal fluids. *Chemical Geology* 184, 37-48.

Drever, J. I. 1974. Geochemical model for the origin of Precambrian banded iron formations. *Geological Society of America Bulletin* 85,1099-1106.

Dumitrica, P. 1973. Cenozoic endoskeletal dinoflagellates in southwestern Pacific sediments cored during Leg 21 of the DSDP. In*:* Burns, R.E., Andrews, J.E., et al. *Initial Reports of the Deep Sea Drilling Project*, vol. XXI. U.S. Gov. Printing Office, Washington D.C, 819-884.

Duncan, R. A., Hooper, P.R., Rehacek, J., Marsh, J.S., Duncan, A.R. 1997. The timing and duration of the Karoo igneous event, southern Gondwana. *Journal of Geophysical Research: Solid Earth (1978–2012)* 102, 18127-18138.

Dürr, H.H., Meybeck, M., Hartmann, J., Laruelle, G.G., Roubeix, V. 2011 Global spatial distribution of natural riverine silica inputs to the coastal zone. *Biogeosciences* 8, 597-620.

Dürr, H.H., Meybeck, M., Dürr, S.H. 2005. Lithologic composition of the Earth's continental surfaces derived from a new digital map emphasizing riverine material transfer. *Global Biogeochemical Cycles* 19, 1-22

Edmond, J.M., Von Damm, K.L., McDuff, R.E., Measures, C.I. 1982. Chemistry of hot springs on the East Pacific Rise and their effluent dispersal. *Nature* 297, 187-191.

Eldhom, O., Coffin, M.F. 2000. Large igneous provinces and plate tectonics. In: Richards, M.A., Gordon, R.G., van der Hilst, R.D. (Eds.) *The history and dynamics of global plate motions Geophys. Monogr.* 121, 309-326.

Ernst, R. E., Buchan, K.L. 2002. Maximum size and distribution in time and space of mantle plumes: evidence from large igneous provinces. *Journal of Geodynamics* 34, 309-342.

Falkowski, P.G., Katz, M.E., Knoll, A.H., Quigg, A., Raven, J.A., Schofield, O., Taylor, F.J.R. 2004. The evolution of modern eukaryotic phytoplankton. *Science* 305, 354-360.

Faure, G., Hurley, P.M., Powell, J.L. 1965. The isotopic composition of strontium in surface water from the North Atlantic Ocean. *Geochimica et Cosmochimica Acta* 29, 209-220.

Fischer, R., Bruno P., Reitner, J. 2000. Organomineralization of cirratulid annelid tubes-fossil and recent examples. *Facies* 42, 35-49.

Gaffin, S. 1987. Ridge volume dependence on seafloor generation rate and inversion using long term sealevel change. *American Journal of Science* 287, 596-611.

Gaillardet, J., Dupré, B., Louvat, P., Allègre, C.J. 1999. Global silicate weathering and CO_2 consumption rates deduced from the chemistry of large rivers. *Chemical Geology* 159, 3-30.

Galy, A., France-Lanord, C., Derry, L.A. 1999. The strontium isotopic budget of Himalayan rivers in Nepal and Bangladesh. *Geochimica et Cosmochimica Acta* 63, 1905-1925.

Gehling, J. G., Rigby, J.K. 1996. Long expected sponges from the Neoproterozoic Ediacara fauna of South Australia. *Journal of Paleontology* 70, 185-195.

Gersonde, R., Harwood, D.M., (Eds.) 1990. Lower Cretaceous Diatoms from ODP Leg 113 Site 693 (Weddell Sea), Part I, *Vegetative Cells* (Ocean Drilling Program, College Station, TX) 113, 365-402.

Ghatak, A., Basu, A.R. 2011. Vestiges of the Kerguelen plume in the Sylhet Traps, northeastern India. *Earth and Planetary Science Letters* 308, 52-64.

Gibson, S. A., Thompson, R.N., Day, J.A. 2006. Timescales and mechanisms of plume–lithosphere interactions: $^{40}Ar/^{39}Ar$ geochronology and geochemistry of alkaline igneous rocks from the Paraná–Etendeka large igneous province. *Earth and Planetary Science Letters* 251, 1-17.

Gladczenko, T. P., Hinz, K., Eldholm, O., Meyer, H., Neben, S., Skogseid, J. 1997. South Atlantic volcanic margins. *Journal of the Geological Society* 154, 465-470.

Gohl, K., Uenzelmann-Neben, G., Grobys, N. 2011. Growth and dispersal of a Southeast African large igneous province. *South African Journal of Geology* 114, 379-386.

Graham, L.E., Wilcox, L.W. 2000. *Algae*. Prentice Hall, Upper Saddle River, NJ, USA

Grenne, T., Slack, J.F. 2003. Paleozoic and Mesozoic silica-rich seawater: Evidence from hematitic chert (jasper) deposits. *Geology* 31, 319-322.

Harper, H. E., Knoll, A.H. 1975. Silica, diatoms, and Cenozoic radiolarian evolution. *Geology* 3, 175-177.

Hart, S.R., 1969. K, Rb, Cs contents with K, Rb, K/Cs ratios of fresh and altered submarine basalts. *Earth Planet. Sci. Lett.* 6, 295-303.

Hart, S.R., Nalwalk, R.J., 1970. K, Rb, Cs, & Sr relationships in submarine basalts from the Puerto Rico trench. *Geochim. Cosmochim. Acta* 34, 145-155.

Hartmann, J., Jansen, N., Dürr, H.H., Harashima, A., Okubo, K., Kempe, S. 2010. Predicting riverine dissolved silica fluxes into coastal zones from a hyperactive region and analysis of their first order controls. *International Journal of Earth Sciences* 99, 207-230.

Harwood, D.M., Nikolaev, V.A. 1995. Cretaceous diatoms: morphology, taxonomy, biostratigraphy. In: Babcock, L.E., Ausich, W.I. (Eds.) *Siliceous Microfossils (Short courses in Paleontology, no. 8)*, The Paleontological Society, Knoxville, Tennessee, 81-106.

Hein, J. R., Parrish, J.T. 1987. Distribution of siliceous deposits in space and time. *Siliceous sedimentary rock-hosted ores and petroleum* 10-57.

Herman, A.B., Spicer, R.A. 1996. Palaeobotanical evidence for a warm Cretaceous Arctic Ocean. *Nature* 380, 330-333.

Herman, A.B., Spicer, R.A. 1997. New quantitative paleoclimate data for the Late Cretaceous Arctic: evidence for a warm polar ocean. *Palaeogeography, Palaeoclimatology, Palaeoecology* 128, 227-251.

Hodson, M.J., White, P.J., Mead, A., Broadley, M.R. 2005. Phylogenetic variation in the silicon composition of plants. *Annals of Botany* 96, 1027-1046.

Hoernle, K., Hauff, F., van den Bogaard, P., Werner, R., Mortimer, N., Geldmacher, J., Garbe-Schöberg, D., Davy, B. 2010. Age and geochemistry of volcanic rocks from the Hikurangi and Manihiki ocean basin flood basalt provinces. *Geochimica et Cosmochimica Acta* 74, 7196-7219.

Holland, H. D. 1984. *The chemical evolution of the atmosphere and oceans*. Princeton University Press, Princeton, New Jersey, 582 p.

Jansen, N., Hartmann, J., Lauerwald, R., Dürr, H.H., Kempe, S., Loos, S., Middelkoop, H. 2010. Dissolved silica mobilization in the conterminous USA. *Chemical Geology*, 270, 90-109.

Jones, Charles E., Jenkyns, H.C., Coe, A.L., Hesselbo, J.D. 1994. Strontium isotopic variations in Jurassic and Cretaceous seawater. *Geochimica et Cosmochimica Acta* 58, 3061-3074.

Jourdan, F., Bertrand, H., Schärer, U., Blichert-Toft, J., Féraud, G., Kampunzu, A.B. 2007. Major and trace element and Sr, Nd, Hf, and Pb isotope compositions of the Karoo large igneous province, Botswana–Zimbabwe: lithosphere vs mantle plume contribution. *Journal of Petrology* 48, 1043-1077.

König, M., Jokat, W. 2010. Advanced insights into magmatism and volcanism of the Mozambique Ridge and Mozambique Basin in the view of new potential field data. *Geophysical Journal International* 180, 158-180.

Krabbenhöft, A., Eisenhauer, A., Böhm, F., Vollstaedt, H., Fietzke, J., Liebtrau, V., Augustin, N., Peucker-Ehrenbrink, B., Müller, M.N., Horn, C., Hansen, B.T., Nolte, N., Wallmann, K. 2010. Constraining the marine strontium budget with natural strontium isotope fractionations ($^{87}Sr/^{86}Sr*$, $\delta\,^{88/86}Sr$) of carbonates, hydrothermal solutions and river waters. *Geochimica et Cosmochimica Acta* 74, 4097-4109.

Larson, R. L. 1991. Latest pulse of Earth: Evidence for a mid-Cretaceous superplume. *Geology* 19, 547-550.

Larson, R.L., Chase, C.G. 1972. Late Mesozoic evolution of the western Pacific Ocean. *Geol. Soc. Am. Bull.,* 83, 3627-3644.

Lazarus, D.B., Kotrc, B., Wulf, G., Schmidt, D.N. 2009. Radiolarians decreased silicification as an evolutionary response to reduced Cenozoic ocean silica availability. *Proceedings of the National Academy of Sciences* 106, 9333-9338.

Louvat, P., Allègre, C.J. 1997. Present denudation rates on the island of Reunion determined by river geochemistry: basalt weathering and mass budget between chemical and mechanical erosions. *Geochimica et Cosmochimica Acta* 61, 3645-3669.

Louvat, P., Allegre, C.J. 1998. Riverine erosion rates on Sao Miguel volcanic island, Azores archipelago. *Chemical Geology* 148, 177-200.

Love, G.D., Grosjean, E., Stalvies, C., Fike, D.A., Grotzinger, J.P., Bradley, A.S., Kelly, A.E., Bhatia, M., Meredith, W., Snape, C.E., Bowring, S.A., Condon, D.J., Summons, R.E. 2009. Fossil steroids record the appearance of Demospongiae during the Cryogenian period. *Nature* 457, 718-721.

Lupton, J. 1998. Hydrothermal helium plumes in the Pacific Ocean. *Journal of Geophysical Research: Oceans (1978–2012)* 103, 15853-15868.

Lupton, J.E., Pyle, D.G., Jenkins, W.J., Greene, R., Evans, L. 2004. Evidence for an extensive hydrothermal plume in the Tonga-Fiji region of the South Pacific. *Geochemistry, Geophysics, Geosystems* 5, 1-18.

Maher Jr, H.D., 2001. Manifestations of the Cretaceous High Arctic large igneous province in Svalbard. *The Journal of Geology* 109, 91-104.

Mahoney, J.J., Storey, M., Duncan, R.A., Spencer, K.J., Pringle, M. 1993. Geochemistry and age of the Ontong Java Plateau. *The Mesozoic Pacific: Geology, Tectonics, and Volcanism, Geophys. Monogr. Ser* 77, 233-261.

Maldonado, M., Carmen Carmono, M., Uriz, M.J., Cruzado, A. 1999. Decline in Mesozoic reef-building sponges explained by silicon limitation. *Nature* 401, 785-788.

Maliva, R. G., Knoll, A.H., Siever, R. 1989. Secular change in chert distribution: a reflection of evolving biological participation in the silica cycle. *Palaios* 4, 519 - 532.

Maloof, A.C., Rose, C.V., Beach, R., Samuels, B.M., Calmet, C.C., Erwin, D.H., Poirier, G.R., Yao, N. and Simons, F.J. 2010. Possible animal-body fossils in pre- Marinoan limestones from South Australia. *Nature Geoscience* 3, 653–659.

Marzoli, A., Renne, P.R., Piccirillo, E.M., Ernesto, M., Bellieni, G., De Min, A. 1999. Extensive 200-million-year-old continental flood basalts of the Central Atlantic Magmatic Province. *Science* 284, 616-618.

McCartney, K., Wise, S.W. 1990. Cenozoic silicoflagellates and ebridians from ODP Leg 113: biostratigraphy and notes on morphologic variability. In: Barker, P.F., Kennett, J.P. et al. (Eds.) *Proc. ODP, Sci. Results* 113, 729-760.

McCartney, K., Harwood, D.M., Witkowski, J. 2010. A rare double skeleton of the silicoflagellate Corbisema. *Journal of Micropalaeontology* 29, 185-186.

McHone, J.G., 2003. Volatile emissions from Central Atlantic Magmatic Province basalts: mass assumptions and environmental consequences. *Geophysical Monograph American Geophysical Union 136, 241-254.*

Medlin, L., Kooistra, W.H.C.F., Gersonde, R., Sims, P.A., Wellbrock, U. 1997. Is the origin of diatoms related to the end-Permian mass extinction? *Nova Hedwigia* 65, 1 -11.

Meybeck, M., 1980. Pathways of major elements from land to ocean through rivers. *Review and Workshop on River Inputs to Ocean Systems, Rome (Italy), 26 Mar 1979*. UN.

Meybeck, M., Ragu, A.1997. River discharges to the oceans: an assessment of suspended solids, major ions, and nutrients. UNEP, 245 p.

Michard, G., Albarède, F., Michard, A., Minster, J-F., Charlou, J-L., Tan, N. 1984. Chemistry of solutions from the 13 N East Pacific Rise hydrothermal site. *Earth and Planetary Science Letters* 67, 297-307.

Moore, M.J., Bell, C.D., Soltis, P.S., Soltis D.E. 2007. Using plastid genome-scale data to resolve enigmatic relationships among basal angiosperms. *Proc. Nat. Acad. Sci.* 104, 19363-19368.

Moshkovitz, S., Erlich, A., Soudry, D., 1983. Siliceous microfossils of the Upper Cretaceous Mishash Formation, Central Negev, Israel. *Cretaceous Res.* 4, 173-194.

Moulton, K. L., West, J., Berner, R.A. 2000. Solute flux and mineral mass balance approaches to the quantification of plant effects on silicate weathering. *American Journal of Science* 300, 539-570.

Müller, R.D., Sdrolias, M., Gaina, C., Steinberger, B., Heine, C. 2008. Long-term sea-level fluctuations driven by ocean basin dynamics. *Science* 319, 1357-1362.

Nakanshi, M., Winterer, E. 1998. Tectonic history of the Pacific-Farallon-Phoenix triple junction from Late Jurassic to Early Cretaceous: An abandoned Mesozoic spreading system in the central Pacific basin. *J. Geophys. Res.* 103, 12453-12468.

Oliva, P., Jérome V., Dupré, B. 2003. Chemical weathering in granitic environments. *Chemical Geology* 202, 225-256.

Oliver, L., Harris, N., Bickle, M., Chapman, H., Dise, N., Horstwood, M. 2003. Silicate weathering rates decoupled from the $^{87}Sr/^{86}Sr$ ratio of the dissolved load during Himalayan erosion. *Chemical Geology* 201, 119-139.

Olson, P., Amit, H. 2015. Mantle superplumes induce geomagnetic superchrons. *Frontiers in Earth Science* 3, 1-11.

Orr, W.N., Conley, S. 1976. Siliceous dinoflagellates in the northeast Pacific rim. *Micropaleontology* 22, 92-99.

Owen-Smith, T. M., Ashwal, L.D., Torsvik, T.H., Ganerød, M., Webb, S.J., Werner, S.C. 2013. Seychelles alkaline suite records the culmination of Deccan Traps continental flood volcanism. *Lithos* 182, 33-47.

Palmer, M. R., Edmond, J.M. 1992. Controls over the strontium isotope composition of river water. *Geochimica et Cosmochimica Acta* 56, 2099-2111.

Pankhurst, R. J., Leat, P.T., Sruoga, P., Rapela, C.W., Márquez, M., Storey, B.C., Riley, T.R. 1998. The Chon Aike province of Patagonia and related rocks in West Antarctica: A silicic large igneous province. *Journal of volcanology and geothermal research* 81, 113-136.

Pankhurst, R. J., Riley, T.R., Fanning, C.M., Kelley, S.P. 2000. Episodic silicic volcanism in Patagonia and the Antarctic Peninsula: chronology of magmatism associated with the break-up of Gondwana. *Journal of Petrology* 41, 605-625.

Parsiegla, N., Gohl, K., Uenzelmann-Neben, G. 2008. The Agulhas Plateau: Structure and evolution of a large igneous province. *Geophysical Journal International* 174, 336-350.

Paytan, A., Kastner, M., Campbell, D., Thiemens, M.H. 2004. Seawater sulfur isotope fluctuations in the Cretaceous. *Science* 304, 1663-1665.

Peterson, K. J., Cotton, J. A., Gehling, J. G., Pisani, D. 2008. The Ediacaran emergence of bilaterians: congruence between the genetic and the geological fossil records. *Philos. Trans. R. Soc. B Biol. Sci.* 363, 1435-1443.

Porter, S. M. 2007. Seawater chemistry and early carbonate biomineralization. *Science* 316, 1302-1302.

Porter, S. M. 2010. Calcite and aragonite seas and the de novo acquisition of carbonate skeletons. *Geobiology* 8, 256-277.

Porter, S.M., Moore, J. L., and Riedman, L.A. In preparation.

Racki, G., Cordey F. 2000 Radiolarian palaeoecology and radiolarites: is the present the key to the past? *Earth-Science Reviews* 52, 83-120.

Rai, J., Garg, R., Khare, N. 2008. Actiniscus pentasterias, an endoskeletal siliceous dinoflagellates from Southern Ocean sediments. *Indian Journal of Marine Sciences* 37, 430-434.

Rigo, M., Preto, N., Roghi, G., Tateo, F., Mietto, P. 2007. A rise in the carbonate compensation depth of western Tethys in the Carnian (Late Triassic): deep-water evidence for the Carnian Pluvial Event. *Palaeogeography, Palaeoclimatology, Palaeoecology* 246, 188-205.

Ritterbush, K.A., Rosas,S., Corsetti, F.A., Bottjer, D.J., West, A.J. 2015. Andean sponges reveal long-term benthic ecosystem shifts following the end-Triassic mass extinction. *Palaeogeography, Palaeoclimatology, Palaeoecology* 420, 193-209.

Rochette, P., Tamrat, E., Féraud, G., Pik, R., Courtillot, V., Ketefo, E., Coulon, C., Hoffmann, C., Vondamme, D., Yirgu, G. 1998. Magnetostratigraphy and timing of the Oligocene Ethiopian traps. *Earth and Planetary Science Letters* 164, 497 - 510.

Ronov, A.B., 1981. The Earth's sedimentary shell (quantitative patterns of its structure, compositions, and evolution) *Internat. Geology Rev.* 24, 1365-1388.

Rothpletz, A. 1896. Über die Flysch-Fucoiden und einige andere fossile Algen, sowie über liasische, Diatomeen führende Hornschwämme Zeitschrift Deutsch Geolog. Geselschaft, 48, 854-914.

Rüth, C., Well, R., Roether, W. 2000. Primordial 3He in South Atlantic deep waters from sources on the Mid-Atlantic Ridge. *Deep Sea Research Part I: Oceanographic Research Papers* 47, 1059-1075.

Sager, W.W. 2005. What built Shatsky Rise, a mantle plume or ridge tectonics? *Geological Society of America Special Papers* 388, 721-733.

Sager, W. W., Kim, J., Klaus, A., Nakanishi, M., Khankishieva, L.M., 1999. Bathymetry of Shatsky Rise, northwest Pacific Ocean: Implications for ocean plateau development at a triple junction. *Journal of Geophysical Research: Solid Earth (1978–2012)* 104, 7557-7576.

Schmidt, A.R., Girard, V., Perrichot, V., Schönborn, W. 2010. Testate amoebae from a Cretaceous forest floor microbiocoenosis of France. *Journal of Eukaryotic Microbiology* 57, 245-248.

Schmidt, K., Koschinsky, A., Garbe-Schönberg, D., de Carvalho, L.M., Seifert, R. 2007. Geochemistry of hydrothermal fluids from the ultramafic-hosted Logatchev hydrothermal field, 15 N on the Mid-Atlantic Ridge: temporal and spatial investigation. *Chemical geology* 242, 1-21.

Sen, G., Chandrasekharam, D. 2011. Deccan Traps Flood Basalt Province: An evaluation of the thermochemical plume model. *Topics in igneous petrology*. Springer Netherlands, 29-53.

Seton, M., Gaina, C. Müller, R.D., Heine, C. 2009. Mid-Cretaceous seafloor spreading pulse: Fact or fiction? *Geology* 37, 678-690.

Seton, M. Müller, R.D., Zahirovic, S., Gaina, C., Torsvik, T., Shephard, G., Talsma, A., Gurnes, M., Tunner, M., Maus, S., Chandler, M. 2012. Global continental and ocean basin reconstructions since 200 Ma. *Earth-Science Reviews* 113, 212-270.

Siever, R. 1992. The silica cycle in the Precambrian. *Geochimica et Cosmochimica Acta* 56, 3265-3272.

Sims, P.A., Mann, D.G., Medlin, L.K. 2006. Evolution of the diatoms: insights from fossil, biological and molecular data. *Phycologia* 45, 361-402.

Siver, P.A., Wolfe, A.P. 2005. Eocene scaled chrysophytes with pronounced modern affinities. *International Journal of Plant Sciences* 166, 533-536.

Sperling, E.A., Robinson, J.M., Pisani, D., and Peterson, K.J. 2010. Where's the glass? Biomarkers, molecular clocks, and microRNAs suggest a 200-Myr missing Precambrian fossil record of siliceous sponge spicules. *Geobiology* 8, 24–36

Steinberg, M. 1981. Biosiliceous sedimentation, radiolarite periods and silica budget fluctuations. *Oceanologica Acta* 4, 149-154.

Tardy, Y., N'kounkou, R., Probst, J-L. 1989. The global water cycle and continental erosion during Phanerozoic time (570 my). *American Journal of Science* 289, 455-483.

Taylor, P. D. 1994. An early cheilosteme bryozoan from the Upper Jurassic of Yemen. (With 4 figures in the text). *Neues Jahrbuch fur Geologie und Palaontologie-Abhandlungen* 191, 331-344.

Tejada, M.L.G., Mahoney, J.J., Duncan, R.A., Hawkins, M.P. 1996. Age and geochemistry of basement and alkalic rocks of Malaita and Santa Isabel, Solomon Islands, southern margin of Ontong Java Plateau. *Journal of Petrology* 37, 361-394.

Tejada, M.L.G., Mahoney, J.J., Neal, C.R., Duncan, R.A., Petterson, M.G. 2002. Basement geochemistry and geochronology of Central Malaita, Solomon Islands, with implications for the origin and evolution of the Ontong Java Plateau. *Journal of Petrology* 43, 449-484.

Timm, C., Hoernle, K., Werner, R., Hauff, F., van den Bogaard, P., Michael, P., Coffin, M.F., Koppers, A. 2011. Age and geochemistry of the oceanic Manihiki Plateau, SW Pacific: New evidence for a plume origin. *Earth and Planetary Science Letters* 304, 135-146.

Tréguer, P. J., De La Rocha, C.L. 2012. The world ocean silica cycle. *Annual review of marine science* 5, 477-501.

Trembath-Reichert, E., Wilson, J.P., McGlynn, S.E., Fischer, W.W. 2015. Four hundred million years of silica biomineralization in land plants. *Proceedings of the National Academy of Sciences* 112, 5449-5454.

Vail, P.R., Mitchum, R.M., Thompson, S. 1977. Seismic stratigraphy and global changes of sea level. *Am. Assoc. Petroleum Geologists Mem.* 26, 83-97.

Van Andel, T. H. 1975. Mesozoic/Cenozoic calcite compensation depth and the global distribution of calcareous sediments. *Earth and Planetary Science Letters* 26, 187-194.

Vinn, O., Mõtus, M-A. 2008. The earliest endosymbiotic mineralized tubeworms from the Silurian of Podolia, Ukraine. *Journal Information* 82, 409-414.

Von Damm, K. L. 1990. Seafloor hydrothermal activity: black smoker chemistry and chimneys. *Annual Review of Earth and Planetary Sciences* 18, 173-204.

Von Damm, K. L. 2000. Chemistry of hydrothermal vent fluids from 9–10 N, East Pacific Rise: "Time zero," the immediate posteruptive period. *Journal of Geophysical Research: Solid Earth (1978–2012)* 105, 11203-11222.

von Strandmann, P.A.E.P., Jenkyns, H.C., Woodfine, R.G. 2013. Lithium isotope evidence for enhanced weathering during Oceanic Anoxic Event 2. *Nature Geoscience* 6, 668-672.

Wheat, C. G., McManus, J. 2005. The potential role of ridge-flank hydrothermal systems on oceanic germanium and silicon balances. *Geochimica et Cosmochimica Acta* 69, 2021-2029.

White, W.M., Tapia, M.D.M., Schilling, J.G., 1979. The petrology and geochemistry of the Azores islands. Contrib. Mineral. Petrol. 69, 201–213.

White, A.F., Blum, A.E. 1995. Effects of climate on chemical weathering in watersheds. *Geochimica et Cosmochimica Acta* 59, 1729-1747.

White, A.F., Blum, A.E., Bullen, T.D., Vivit, D.V., Schulz, M., Fitzpatrick, J. 1999. The effect of temperature on experimental and natural chemical weathering rates of granitoid rocks. *Geochimica et Cosmochimica Acta* 63, 3277-3291.

Wilson, P.A., Norris R.D. 2001. Warm tropical ocean surface and global anoxia during the Mid-Cretaceous period. *Nature* 412, 425-429.

Won, M-Z, Below, R. 1999. Cambrian Radiolaria from the Georgina Basin, Queensland, Australia. *Micropaleontology* 45, 325-363.

Xiao, S., Hu, J., Yuan, X., Parsley, R.L., Cao, R. 2005. Articulated sponges from the Lower Cambrian Hetang Formation in southern Anhui, South China: their age and implications for the early evolution of sponges. *Palaeogeography, Palaeoclimatology, Palaeoecology* 220, 89 – 117.

Yin, Z., Zhu, M., Davidson, E.H., Bottjer, D.J., Zhao, F., Tafforeau, P. 2015. *Proc. Nat. Acad. Sci.* 112, E1453-E1460.

Zhang, X-g, Pratt, B.R. 1994. New and extraordinary Early Cambrian sponge spicule assemblage from China. *Geology* 22, 43-46.

Zhu, D-C, Chung, S-L, Mo, X-X, Zhao, Z-D, Niu, Y, Song, B., Yang, Y-H. 2009. The 132 Ma Comei-Bunbury large igneous province: Remnants identified in present-day southeastern Tibet and southwestern Australia. *Geology* 37, 583-586.

Appendix

Faure et al. 1965 $^{87}Sr/^{86}Sr$ model

$$\left[\frac{^{87}Sr}{^{86}Sr}\right]_{SW} = \left[\frac{^{87}Sr}{^{86}Sr}\right]_{v} v + \left[\frac{^{87}Sr}{^{86}Sr}\right]_{s} s + \left[\frac{^{87}Sr}{^{86}Sr}\right]_{m} m_o$$

$$\left[\frac{^{87}Sr}{^{86}Sr}\right]_{SW} = Av + Bs + Cm_o$$

$\left[\frac{^{87}Sr}{^{86}Sr}\right]_{v} = 0.7040$ Strontium isotope ratio of volcanics

$\left[\frac{^{87}Sr}{^{86}Sr}\right]_{s} = 0.7200$ Strontium isotope ratio of silicic continental rocks

$\left[\frac{^{87}Sr}{^{86}Sr}\right]_{m} = 0.7080$ Strontium isotope ratio of marine carbonates

v = the fraction of Sr from volcanics (MORB, OIB, IAM)

s = the fraction of Sr from weathering silicic continental rocks

m_o = the weathering of Phanerozoic marine carbonates

m_o is a constant that varies between 0.6 – 0.8

m_o = 1- v – s

Brass (1976) concluded that strontium from the weathering of marine Carbonates amounts to 75% (0.75) of the total strontium entering the oceans.

Derivation to solve for *v*:

$$\left[\frac{^{87}Sr}{^{86}Sr}\right]_{SW} = Av + Bs + Cm_o$$

$$s = 1 - m_o - v$$

$$\left[\frac{^{87}Sr}{^{86}Sr}\right]_{SW} = Av + B(1 - m_o - v) + Cm_o$$

$$\left[\frac{^{87}Sr}{^{86}Sr}\right]_{SW} = Av + B - Bm_o - Bv + Cm_o$$

$$\left[\frac{^{87}Sr}{^{86}Sr}\right]_{SW} = (A - B)v + B(1 - m_o) + Cm_o$$

$$v = \frac{\left[\frac{^{87}Sr}{^{86}Sr}\right]_{SW} - Cm_o - B(1 - m_o)}{(A - B)}$$

Example for solving *v*:

$$v = \frac{\left[\frac{^{87}Sr}{^{86}Sr}\right]_{SW} - Cm_o - B(1 - m_o)}{(A - B)}$$

$$\left[\frac{^{87}Sr}{^{86}Sr}\right]_{SW} \text{ at } 0\text{Ma} = 0.70918$$

$$v = \frac{0.70918 - 0.7080(0.6) - 0.7200(1 - 0.6)}{0.7040 - 0.7200}$$

$$v = \frac{0.70918 - 0.4248 - 0.288}{-0.016}$$

$$v = \frac{-0.00182}{-0.016}$$

$$v = 0.22625$$

$$s = 1 - 0.6 - 0.22625$$

$$s = 0.17375$$

Brass 1976 $^{87}Sr/^{86}Sr$ model

$$\frac{dR_{SW}}{dt} = (R_{ls} - R_{SW})\frac{\{Sr\}_{ls}}{\{Sr\}_{SW}}\left(\frac{(1-X)F}{V}\right) + (R_{CC} - R_{SW})\frac{\{Sr\}_{CC}}{\{Sr\}_{SW}}\left(\frac{F(X)}{V}\right) + (R_{MORB} - R_{SW})\frac{\{Sr\}_{MORB}}{\{Sr\}_{SW}}\left(\frac{G}{V}\right)$$

$\frac{dR_{SW}}{dt}$ = the rate of change in the $^{87}Sr/^{86}Sr$ curve in 10 million year intervals

R_{ls} = the $^{87}Sr/^{86}Sr$ value of riverine water draining carbonates

R_{SW} = the $^{87}Sr/^{86}Sr$ value of modern day seawater

$\{Sr\}_{ls}$= the concentration of strontium in riverine water draining carbonates

$\{Sr\}_{SW}$= the concentration of strontium in modern day seawater

X= the fraction of the global riverine flux from rivers draining non-carbonates

F= global continental runoff

V = the volume of the ocean today

R_{CC}= the $^{87}Sr/^{86}Sr$ value of rivers draining non-carbonates

$\{Sr\}_{CC}$= the concentration of strontium in rivers draining non-carbonates

R_{MORB}= the $^{87}Sr/^{86}Sr$ value of hydrothermal fluids

G= the flux of water that circulates through the oceanic crust